2-8-2016 12:00 AM

Wind Loading on Full-scale Solar Panels

Zeinab Samani
The University of Western Ontario

Supervisor
Horia Hangan
The University of Western Ontario Joint Supervisor
Girma Bitsuamlak
The University of Western Ontario

Graduate Program in Civil and Environmental Engineering
A thesis submitted in partial fulfillment of the requirements for the degree in Master of Science

Abstract

Wind load governs the design of supporting structures of solar panels and constitutes approximately fifty percent of the total cost. There are various test scale related issues while testing solar panels (small structures) in boundary layer wind tunnel laboratories meant for tall buildings (large structures). Emergence of large testing facilities, however, is enabling testing full-scale solar panels. In this thesis an extensive experimental program is conducted at WindEEE Dome using full-scale solar panels and finite element modeling. The experimental program includes: (i) high resolution pressure tests to understand the sensitivity of pressure taps density and distribution; (ii) force balance test to determine the reactions of the solar panel under wind loading accounting for aeroelastic effects and validate pressure test results; (iii) finite element modeling to assess the internal stress of the solar rack elements and improvement of the rack cross section.

Study of pressure tap layout and resolution illustrated that a fairly high density resolution is required to capture all the aerodynamic features of pressure on the solar panel surfaces. It is found that the uplift force obtained from the force balance tests are larger compared to the pressure taps as result of the dynamic effects of wind loading. The finite element analysis of solar racks was performed using the experimentally established wind loading data, which includes all dynamic features of the forces obtained from the force balances. It is concluded that the solar rack cross sections can be structurally optimized and there is a possibility to save in aluminum elements up to 40%.

Keywords

Full-Scale Solar Panel, Experimental Analysis, Wind Testing, WindEEE Dome, Finite Element Analysis

Co-Authorship Statement

This thesis has been produced in accordance with the guidelines of the School of Graduate and Postdoctoral Studies. All the experiments, numerical modeling, calibration, interpretation of results and writing the draft and final version of thesis were carried out by the candidate herself, under the supervision of Prof. Horia Hangan and Prof. Girma Bitsuamlak. The supervisors' contribution consisted of providing advice throughout the research program and reviewing the draft and the final thesis as well as the results of this research.

Acknowledgments

I would like to express my appreciation to the people who have supported me through this research and have been essential to its completion.

I am extremely thankful and indebted to my supervisors Prof. Horia Hangan and Prof. Girma Bitsuamlak who have been invaluable in providing assistance, guidance and recommendations along the way. Their constant technical and motivational supports were unforgettable for me.

Sincere thanks to the manager of German Solar Corporation, Mr. Dennis German, for providing the opportunity and funding of this interesting project.

I am so grateful to employees and fellows of the WindEEE Gerry Dafoe, Andrew Mathers, and Adrian Costache and Dr. Maryam Refan, who have tirelessly assisted me in this project.

A special thanks to Dr. Ahmad Elatar and Dr. Chowdhury Mohammad Jubayer, Tibebu Birhane who shared their feedback, guidance, assistance and support during this research.

I would like to thank my other friends and staff at the Wind Engineering, Energy and Environment (WindEEE) Research Institute and Boundary Layer Wind Tunnel Laboratory for their support especially Mahshid Nasiri, Djordje Romanic, Ryan Kilpatrick and Dan Parvu for all their helps.

To my parents, for their unceasing encouragement, support and affections. I am proud to be your daughter and fully indebted to you because of your dedications and self-sacrifice throughout my life.

Last but certainly not the least, a great gratitude to my wonderful husband, Dr. Bahman Daee. I will always remember how he helped me these years. Without his patience, understanding, encouragements, and supports none of my achievements would be possible.

Table of Contents

List of Tables

List of Figures

List of Appendices

Nomenclature

A_0	Reference area for calculating M for an inclined panel (m^2)
A_i	Tributary area associated with $P_{net,i}$ (m^2)
A_{Drag}	Area of module projected onto a vertical plane (m^2)
A_{Uplift}	Area of module projected onto a horizontal plane (m^2)
$A_{downforce}$	Area of module projected onto the horizontal plane (m^2)
C_D	Drag coefficient
Ce	Exposure coefficient
C_P	Pressure coefficient
C_{peq}	Equivalent pressure coefficient
C_{plower}	Pressure coefficient of the lower surface of the panels
C_{pmax}	Maximum pressure coefficient
C_{pmean}	Mean pressure coefficient
C_{pmin}	Min pressure coefficient
C_{pnet}	Net pressure coefficient
C_{pupper}	Pressure coefficient of the upper surface of the panels
$(CpCg)_{drag}$	Absolute pressure coefficient
$(CpCg)_{downforce}$	Absolute value of uplift pressure coefficient
$(CpCg)_{moment}$	Moment coefficient
$(CpCg)_{uplift}$	Absolute pressure coefficient
C_L	Lift coefficient
C_M	Moment coefficient
C_N	Coefficient of net area weighted average pressure from both upper and lower surfaces of the panel
f	Frequency (Hz)
F	Aerodynamic wind force (N)
F_D	Drag force (N)
F_L	Lift force (N)
F_x	Drag force (N)
$F_{x,peak}$	Peak wind load in x direction (N)
F_z	Lift force (N)
$F_{z,min,peak}$	Min peak wind load in z direction (N)

$F_{z,max,peak}$	Max peak wind load in z direction (N)
F_t	Total aerodynamic wind force (N)
G	Gust factor
H	Height of the panel (m)
h	Mean roof height (m)
i	Tap number
L	Horizontal dimension of building which measured in along wind angle of attack (m)
L_m	Moment arm (m)
L_P	Width of the panel (m)
M	Overturning moment (N-m)
P	Pressure on the surface of the panels (Pa)
P_0	Reference pressure (Pa)
P_{eq}	Equivalent pressure (Pa)
$P_{net,i}$	Net pressure at the specific i tap number on the panel (pa)
q	Dynamic pressure (Pa)
qh	Velocity pressure calculating at mean roof height h
R	Resolution
Re	Reynolds number
U	Mean wind speed (m/s)
u*	Friction velocity (m/s)
V	Free stream velocity (m/s)
V_z	Mean velocity at height z (m/s)
V_0	Reference fluid velocity (m/s)
Z	Height (m)
Z_0	Surface roughness

Greek Symbols

ρ	Density of air (kg/m^3)
θ	Panel inclination angle (^{o})
μ	Dynamic viscosity of the air (Pa.s)
Φ	Aluminum resistance factor

Abbreviations

ABL	Atmospheric Boundary Layer
AOA	Angle Of Attack
ASCE	American Society of Civil Engineers
BLWT	Boundary Layer Wind Tunnel
CFD	Computational Fluid Dynamics
CSI	Computers and Structures, Inc.
DAQ	Data Acquisition
DC	Direct Current
DES	Detached Eddy Simulation
ESDU	Engineering Sciences Data Unit
FE	Finite Element
FEA	Finite Element Analysis
FEM	Finite Element Model
NBCC	National Building Code of Canada
NIDS	National Instruments Data acquisition System
PV	Photovoltaic
RANS	Reynolds-Averaged Navier-Stokes
SAP	Structural Analysis Program
WindEEE	Wind Engineering, Energy and Environment

Chapter 1

1 Introduction

Solar energy is a renewable and clean energy which is a sustainable alternative to fossil fuels, from an environmental perspective. One of the current technologies to harness solar energy is to use solar cells attached on panels (hence referred as solar panels) which convert the solar radiation into electricity. During the past decade, many researchers have attempted to improve thier power generation efficiency to make it competitive with conventional sources of energy. Despite the environmental advantages of solar energy and the rapid development of solar plants, there are some difficulties which hinder their vast implementation. The main obstacle of using solar panels in industrial scale is the initial capital. The cost of supporting structure of solar panels is a significant portion of the total cost. Therefore, section size optimization of the supporting structure is essential in order to reduce the initial cost of solar panels. Wind load governs the design of supporting structures of solar panels. Due to lack of accurate design code, most designers typically follow the design procedures recommended by building codes meant for large sloped roofs. This may lead to conservative results in some cases and unsafe designs in others cases. Moreover, the lack of appropriate wind design guidelines is also slowing down their wide applications.

Wind load can be reasonably determined by performing a series of experiments on a reduced model-scale solar panel using wind testing facilities such as the Boundary Layer Wind Tunnel (BLWT). The boundary layer wind tunnel testing is a widely accepted method, especially for large structures such as tall buildings at small-scale. The boundary layer wind tunnel testing guidelines set by American Society of Civil Enginering (ASCE) requires that the projected area of the model should be less than 8% of the wind tunnel cross sectional area to avoid the blockage effects on the results. Therefore, a full-scale test of a solar panel in the typical wind tunnels is not possible due to the blockage restrictions. Large number of wind tunnel studies on single solar panel and arrays were conducted in wind tunnel to produced aerodynamic databases. There are some scale related issues that require further investigation in wind testing facility e.g. scale effects, dynamic effects, pressure tap distribution resolution effects. However, testing small structures in a wind

tunnels is not practically possible as they are typically designed to test tall buildings at a scale of 1:300 to 1:500. The newly constructed Wind Engineering Energy and Environment Research Institute that housed the WindEEE Dome has the capability of testing large scale structural models. Thus, full-scale testing of a solar panel becomes feasible.

1.1 WindEEE Dome

WindEEE Dome laboratory is used in the present study to perform the wind experimentation on full-scale solar panels. This laboratory is capable of simulating different wind flow systems such as tornado, downburst, gust front and low level nocturnal currents. WindEEE Dome is hexagonal in shape and with inner wall to wall distance of 25 m (outer wall to outer wall of 40 m distance) and 3.8 meters test chamber height. One of the six peripheral walls of the WindEEE has a matrix of 60 fans (4 rows of 15 fans each) (Hangan, 2014). The fans on this wall, operate in conjunction with two sets of contraction side walls and provide “wind-tunnel type” flows at a large scale. The contraction walls form a funnel shape cross section for the wind flow, approximately tapering from 14m to 5m in width within 10m length and 3.8m height (Figure 1.1). These fans are capable of simulating a multi-scale atmospheric conditions which were used in this study to test the full-scale solar panels.

The WindEEE Dome’s large size allows for wind simulation in an extended area with a complex and adjustable terrain. In WindEEE Dome the inflow and boundary conditions can be manipulated to reproduce the dynamics of real wind systems at large scales and under controlled conditions. Owing to the large space in this new facility, wind testing on large elements such as full-scale solar panel, small wind turbine and large wind turbine blades is possible (Hangan 2010).

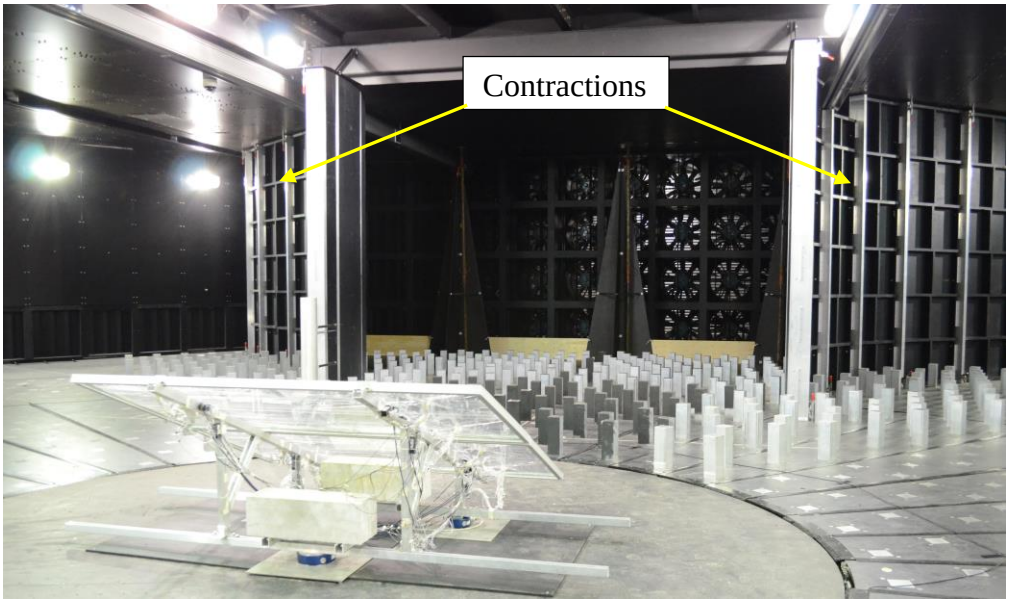

Figure 1.1: View of contractions at WindEEE Dome used for the experiments

1.2 Wind pressure measurements

Once wind impinges on an inclined solar panel, it separates at the leading edges and flows around it and induces unequal pressure on its upper and lower surfaces. The surface pressure on an object is usually expressed in terms of a dimensionless wind pressure parameter that is referred as coefficient of pressure (C_P) and is defined as:

$$C_P = \frac{P - P_0}{\frac{1}{2}\rho v_0^2} \tag{1.1}$$

where, P is the static pressure on the surface (Pa), P_0 is the pressure at a reference point without the influence of the body (Pa), ρ is the density of the fluid (kg/m^3) and V_0 is the fluid velocity at reference point (m/s).

The surfaces of the solar panels are exposed to two dynamic forces, drag force in the direction of wind flow and lift force in the direction perpendicular to the flow. The drag (F_D) and lift (F_L) forces can be calculated using Equations 1.2 and 1.3. Aerodynamic forces on an inclined flat plate are shown in Figure 1.2.

$$F_D = \frac{1}{2}\rho v_0^2 C_D \quad (1.2)$$

$$F_L = \frac{1}{2}\rho v_0^2 C_L \quad (1.3)$$

where C_D and C_L are lift and drag coefficients which are the components of C_p in drag and lift directions, respectively. If the surface of the object is divided in to *i* smaller areas, the relation of F_D and F_L with total wind force (F) is given by the following equations:

$$F = \sum_{i=1}^{n} p_{net,i} \times A_i \quad (1.4)$$

$$F_D = \sum_{i=1}^{n} p_{net,i} \times \sin\theta \times A_i \quad (1.5)$$

$$F_L = \sum_{i=1}^{n} p_{net,i} \times \cos\theta \times A_i \quad (1.6)$$

where, $P_{net,i}$ is the pressure at a specific location on the panel, A_i is the tributary area (see figure 1.3) associated with $P_{net,i}$ (m^2) and θ is the inclination angle (^{o}).

A moment is expressed as the product of force and the displacement vector with respect to a reference point from the point where the force is applied. Thus, a moment coefficient is used to express the overturning component of wind loading. Definition of overturning moment (M) is given in Equation 1.7:

$$M = \frac{1}{2}\rho v_0^2 C_M A_0 L_m \quad (1.7)$$

where, M is the overturning moment about the center axis of the plate (N-m) (Figure 1.2) and L_m is moment arm (m).

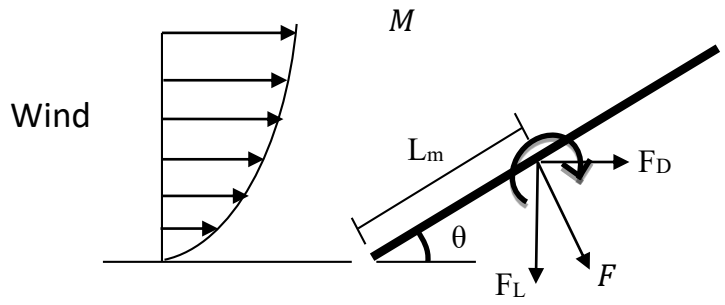

Figure 1.2: Aerodynamic forces on an inclined flat plate

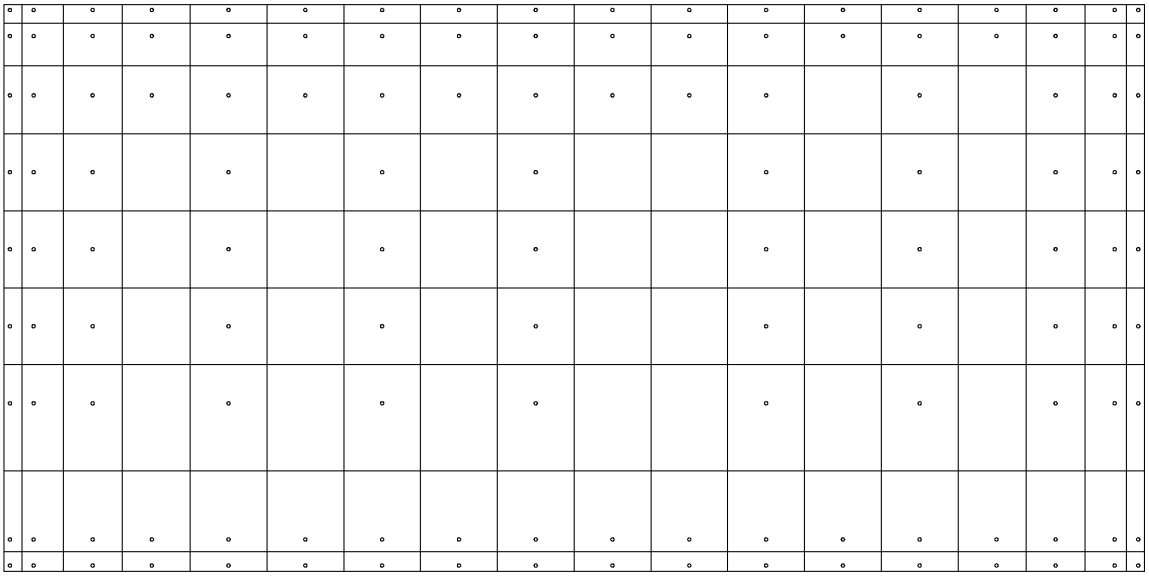

Figure 1.3: Tributary area of each taps

1.3 Literature review

Based on the mounting location, solar panels can be categorized into two major classes; roof mounted and ground mounted. Figure 1.4 and Figure 1.5 display typical view of roof mounted and ground-mounted solar panels, respectively.

Figure 1.4: Typical view of roof-mounted solar panels

Figure 1.5: Typical view of ground-mounted solar panels

Ground mounted PV modules, which are the subject of this study have several advantages over roof mounted systems. Ground mounted solar panels are independent of the roof pitch and orientation and their installation does not affect the structural design of the main building. There is more air circulation around ground-mounted panels which keeps them cooler and accessible for maintenance and cleaning. Therefore, there is a tendency toward using ground-mounted panels in utility scale plants.

The number of studies conducted for ground mounted solar panels are very limited due to the fact that the wind tunnel testing of ground mounted solar panels is challenging. Boundary layer wind tunnels are usually designed for wind testing at scales of the order of 1:100 or smaller. While for simulation of ground-mounted solar panel at larger scales (e.g. 1:30), 10 meters of the atmospheric boundary layer (ABL) needs to be modeled which is not possible in common testing facilities. Therefore, most of experimental studies were

conducted on small-scale models of panels and therefore might not capture all the dynamic effects of wind on a panel. Nevertheless, there are efforts that looked into ground mounted solar array testing such as Kopp et al. (2012) and Warsido et al. (2014).

Shademan and Hangan (2010) carried out a computational fluis dynamics (CFD) simulation on ground mounted solar panels in 3x4 arrangement at different wind angles of attack. The results of this study illustrated that the entire structure experience the largest wind loading at 0^0 and 180^o wind angle of attack, while 150^o causes the most critical fluctuating resultant.

Bitsuamlak et al. (2010) conducted a research on ground mounted stand-alone and arrayed solar panels by using Computational Fluid Dynamics (CFD) method in order to investigate the aerodynamic features of a PV systems. In this study, it was shown that the pressure coefficient distribution obtained from numerical modeling is underestimated compared to full-scale experimental results. Moreover, when solar panels are placed in a row, sheltering effect from upwind solar panels decreases wind loads on adjacent panels. The authors also concluded that the solar arrays experienced the greatest wind load at 180^0 wind angle of attack.

Kopp et al. (2012) studied wind loading on the ground mounted array to illustrate the effect of the building on pressure distribution of the roof mounted solar arrays. This study was performed at the Boundary Layer Wind Tunnel II (BLWT II) at the University of Western Ontario. It was found that there was a considerable difference in aerodynamics loading between ground mounted and roof mounted solar panel arrays as a result of the interaction of the flow with the building itself.

Aly and Bitsuamlak (2013) conducted wind tunnel tests on a stand-alone ground mounted solar panel of five different geometric scales (1:50, 1:30, 1:20, 1:10 and 1:5) with 25^o and 40^o tilt angles. In this study the impact of different scales on wind loading on the panel was analyzed and a CFD study was performed on 1:50, 1:20 and 1:10 geometric scales with 40^o tilt. It was observed that the mean surface pressures on the panel was not significantly influenced by the different scales. However, standard deviation and peak pressure coefficients correlated with geometric scales. The 3-s peak load was found similar in all

scales except for 1:50 scale, which was very close to the ground. It was then concluded that once peak values of the loading is the target of study, large model of ground-mounted panel can be subjected to low turbulence wind flow.

Stathopoulos et al. (2014) examined the wind loads on a stand-alone solar panel placed on ground, flat roof, and gable roof of a building. It was demonstrated that the wind angles of attack in the range of 105^o to 180^o cause the extreme pressure coefficient values with a maximum effect at 135^o. The authors also assessed various geometries and concluded that the effect of building height and panel location were not significant for the roof-mounted systems and the effect of panel inclination is significant only for the critical wind angle of attack. However, when the panel is ground mounted, the minimum and maximum peak pressure coefficients were occurred at 30^o and 135^o wind angles of attack, respectively. The 45^o inclination angle of the panel resulted in both maximum and minimum peak pressures.

Warsido et al. (2014) conducted wind tunnel testing and investigated the effect of row spacing on wind loads for a solar panel mounted on both flat roof and ground. The testing was performed on 1:30 geometric scale model with inclination of 25^o and wind angles of attack ranging from 0^o to 180^o at 10^o intervals. They found that the influence of lateral spacing between panels on the inner panel rows of the ground mounted system was negligible. However, the wind loads were found greater on the outer rows for the zero lateral spacing case. It was concluded that as longitudinal spacing between panels was increased wind loads on the panels intensified. Moreover, it was shown that the isolated panels experienced higher wind pressure compare to those placed in an array configuration.

Shademan et al. (2014a) conducted a research on ground mounted solar panels in both stand-alone and array configuration with a tilt angle of 45^o. In this study CFD simulations using 3D steady Reynolds-Averaged Navier-Stokes (RANS) were performed to investigate the effect of wind loading. Wind angles of attack ranging from 0^o to 180^o at 30^o intervals were employed and the influence of spacing between individual modules and ground clearance was studied.

The results of this study illustrated that increasing the spacing between individual modules increased the loading close to the gap. Increasing the ground clearance also resulted in higher wind loads.

Shademan et al. (2014b) furthered the investigation on the ground mounted solar panel using Detached Eddy Simulation (DES). It was reported that as the ground clearance increased, stronger vortex shedding and larger unsteady forces were observed.

Jubayer et al. (2014) performed 3D unsteady Reynolds-Averaged Navier-Stokes (RANS) to find the effect of wind load on the ground mounted stand-alone photovoltaic (PV) panel with 25 degree inclination. The authors illustrated that mean pressure coefficients of the solar panel surfaces are in a good agreement with the experimental results of wind tunnel test by Abiola-Ogedengbe (2013). The results of this study also demonstrated that the maximum uplift occurs at 180^o wind angle of attack while 45^o and 135^o are more critical for overturning.

Abiola-Ogedengbe et al. (2015) investigated the pressure distribution on a scaled model of ground mounted solar panel with 25^o and 40^o inclination and measured wind profiles at 0^o, 30^o, 150^o and 180^o of wind angle of attack. In this study, it was concluded that in an open terrain exposure the wind pressure is more critical for smoother exposures (less roughness). The 25^o inclination of the panel was found to produce larger loading in comparison with the 40^o case. It was also noted that the gap between upper and lower panels play an important role in pressure distribution and should be considered in structural design of the panel. For Reynolds number once Reynolds number is greater than $2x10^4$, the authors also experimentally confirmed that pressure coefficient is independent of the Reynolds number. This result was in compliance with the results achieved by Hosoya et al. (2008) and Aly et al. (2014).

1.4 Motivations

The main obstacle in production of solar panels in industrial scale is the initial capital. The cost of supporting structure of solar panels is a significant portion of the total cost. Therefore, section improvement of this structural element is essential in order to reduce the

manufacture cost of solar panels. Wind load governs the design of supporting structures of solar panels and due to limited aerodynamic data and design codes, most of designers typically follow the conservative design procedures recommended for other similar structures by Engineering Standards in order to find the maximum wind load on the solar panels.

The National Building Code of Canada (NBCC 2010) National Building Code of Canada (NBCC, 2010) currently does not provide specific guideline for determination of wind loading on ground-mounted solar panels. In current practice, the designers of solar panel select the pressure coefficients based on their interpretation from the code by using similar geometries outlined in NBCC 2010. Due to the lack of a unique applicable standard for wind load estimation on solar panels in Canada, most of the designers refer to ASCE 7-10 which specifies pressure coefficients of mono-slope free roofs for different elevations with respect to the ground levels. However, it is currently unclear to what extent the minimum design load for mono-slope free roofs are applicable to ground mounted stand-alone solar panels. We acknowledge the various efforts by various groups in codification of wind load on solar panels based on the studies reviewed in this study and others. However there are clear limitations in full-scale wind study for solar-panel.

Hence, to bridge the gap between the current practice and inadequate applicable standards, an accurate research was required in order to determine wind pressure distribution on a real solar panel. Although several past studies estimated wind loads on solar panels for different geometries, this research is pioneer in performing wind testing on a full-scale solar panel under a realistically simulated turbulent ABL flow. Implementation of a full-scale model of a solar panel which was fully utilized with pressure taps and force balances could comprehensively capture the details of wind effects on the panel and internal forces in the supporting structure members.

1.5 Objectives

Therefore, the main objectives of this research are in two folds: structural analysis of supporting members of solar panels and studying the aerodynamics of these panels using

full scale experimental tests by employing the multi-fan capability of WindEEE. Once this is achieved the following sub-objectives are followed:

1. Conduct wind testing on full-scale panel with high-resolution pressure taps distribution to determine an accurate wind loading on a ground-mounted panel;
2. Achieve the maximum support reactions of the solar rack to be employed for finite element simulation, stresses analysis, and design purposes;
3. Develop and calibrate a 3D Finite Element (FE) model of the solar panel using (SAP 2000);
4. Design of the supporting structure of the solar panel by employing the results of previous steps.

It is hypothesized that through accurate wind load evaluation and design improvement of the support members, the overall cost of the installed solar panel could be reduced. Thus making this renewable source of energy more competitive.

1.6 Organization of the thesis

Chapter 2 presents the test set up and methodology. Chapter 3 discusses aerodynamic and aero-elastic data analysis. Chapter 4 presents the FEA and chapter 5 summarizes the conclusion of this study.

Chapter 2

2 Test set-up and methodology

2.1 Background

In this research, an extensive experimental work is carried out on a full-scale, stand-alone, ground-mounted gravity solar panel at the WindEEE Dome. The aim of the study is to measure the wind pressure distribution on a solar panel and to accurately evaluate the maximum internal forces of the supporting structure under wind loading. A wind profile corresponding to the open terrain exposure is achieved after various trial and error efforts at the WindEEE Dome, as described in Section 2.2. This wind profile is compared and calibrated with a benchmark target wind profile prescribed in the (Engineering Sciences Data Unit (ESDU) similar to the practice in the boundary layer wind tunnels.

With the collaboration of "German Solar Corporation", two types of test models inclined at 25^{o} are prepared for the experimental program, which are described in detail in Section 2.3. The first model consists of a supporting structure similar to the real solar panel, and a double layer clear sheet made of rigid Polycarbonate as a replacement of the real panel. This double layer Polycarbonate sheet is instrumented by using pressure taps in order to record the time history of wind pressure on the solar panel. The results of wind pressure on this model is elaborated in Chapter 3. The second model is a full-scale solar panel, fabricated with the same material and elements of a real solar panel. This model is mounted on three force balances in order to monitor its reactions under a real wind loading profile. Under the wind loading, the support reactions of this model is recorded, analyzed and further used for Finite Element Analysis conducted on supporting structure, as described in Chapter 4. The second model in fact represents full-scale aero-elastic model testing. The data acquisition system, test set-up and the instrumentation of models are explained further in this chapter.

2.2 Boundary layer development at WindEEE

The wind testing is carried out for two wind profiles. The first wind profile is an open terrain boundary layer with a velocity of 56.2 km/h (which is equivalent with 50% fans

speed at WindEEE). The roughness of the boundary layer velocity profile (Z_0) is selected equal to 0.01 which is the maximum practical roughness value at WindEEE which can be achieved with high accuracy. The second profile is a uniform profile with 59 km/h velocity (which is equivalent to 50% of fans speed at WindEEE). The mean wind speed in WindEEE represents the velocity of the wind at 1m above the floor, measured with Pitot tube at a distance approximately 10 meters away from the fans.

In order to obtain the wind profile corresponding to the open terrain exposure, several passive flow conditioning elements are used in the inlet section of the 60 fan wall in WindEEE. These elements include three isosceles triangular spires, rectangular roughness blocks on the floor of the WindEEE test chamber and the contraction, as described in Figure 2.1. Numerous trial and error and numerical analysis are undertaken by an expert team at WindEEE in order to achieve the target atmospheric boundary layer (ABL) matching with those prescribed in ESDU (Engineering Sciences Data Unit, ESDU 82026 & ESDU 83045) for boundary layer flow. In each attempt, several parameters such as speed of fans, the pattern of operating fan, roughness, flow condition elements, etc. are systematically changed to obtain a matching profile.

Ultimately, the ensuing wind velocity profile closely matches the mean wind velocity profile for an open terrain exposure obtained from the ESDU (Engineering Sciences Data Unit) using Equation 2.1:

$$V_z = 2.5u^* \times \ln(z/z_0) \qquad (2.1)$$

where V_z is mean velocity at height z, u* is friction velocity, z_o is surface roughness parameter and z is height.

A second profile for uniform flow is obtained without the ground roughness elements. This is done to compare the effects of the ground roughness on the wind load on the solar panel for both boundary layer and uniform flow. Figure 2.2 and Figure 2.3 compare the boundary layer mean wind velocity and turbulence intensity profiles obtained at WindEEE with those described in ESDU. Both Figures 2.2 and 2.3 show a fair agreement between the two sets

of data, at least for a meter above the ground, which is corresponding to the panel immersion in the boundary layer.

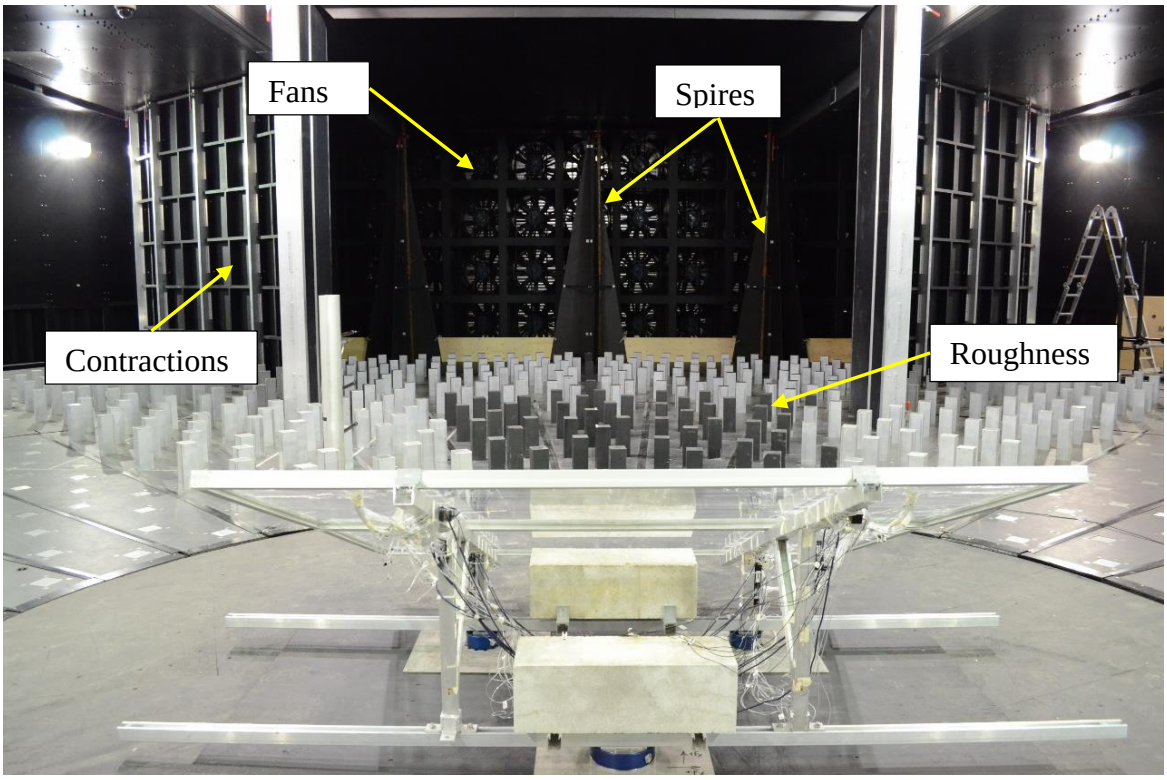

Figure 2.1: View of passive flow conditioning elements at WindEEE used for the experiments

Figure 2.4 compares the turbulence velocity spectrum of WindEEE with ESDU standard at the solar panel height, H = 0.96 m. As it can be seen from Figure 2.4, the slope of the spectra is preserved, but the measured spectra are shifted, towards high frequency for stream-wise velocity compared to the ESDU spectrum. This is a typical feature for all boundary layer wind tunnels for large scale testing. In this experiment, Reynolds number based on the wind speed at the solar panel height, H = 0.96, the breadth of the panel (B=1.99m) and the air properties at 20^{oC}, is evaluated to be 2.11×10^{6} and 2.21×10^{6} for boundary layer and uniform flow, respectively.

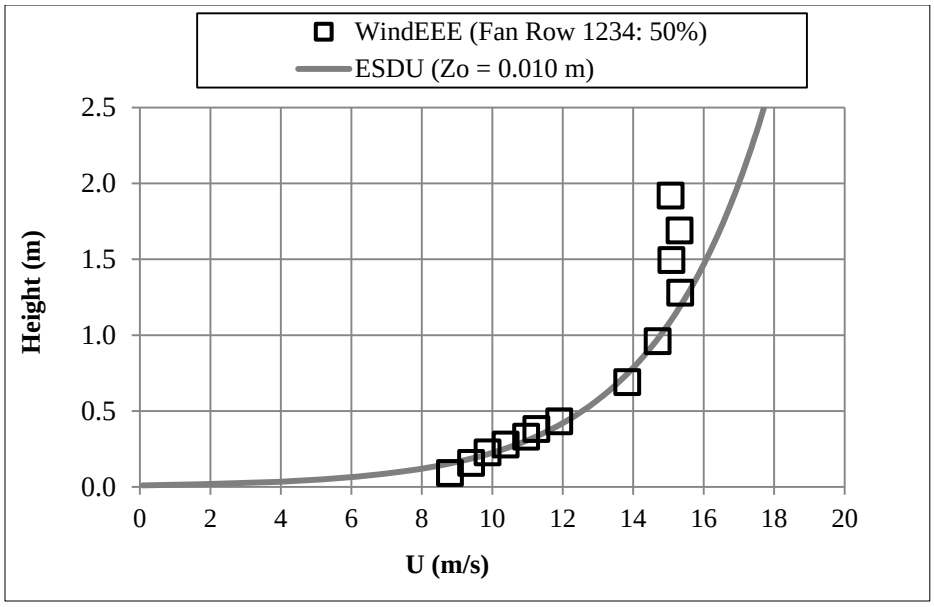

Figure 2.2: Comparison of mean wind velocity profile measured at WindEEE and ESDU standard for open terrain with Zo=0.01

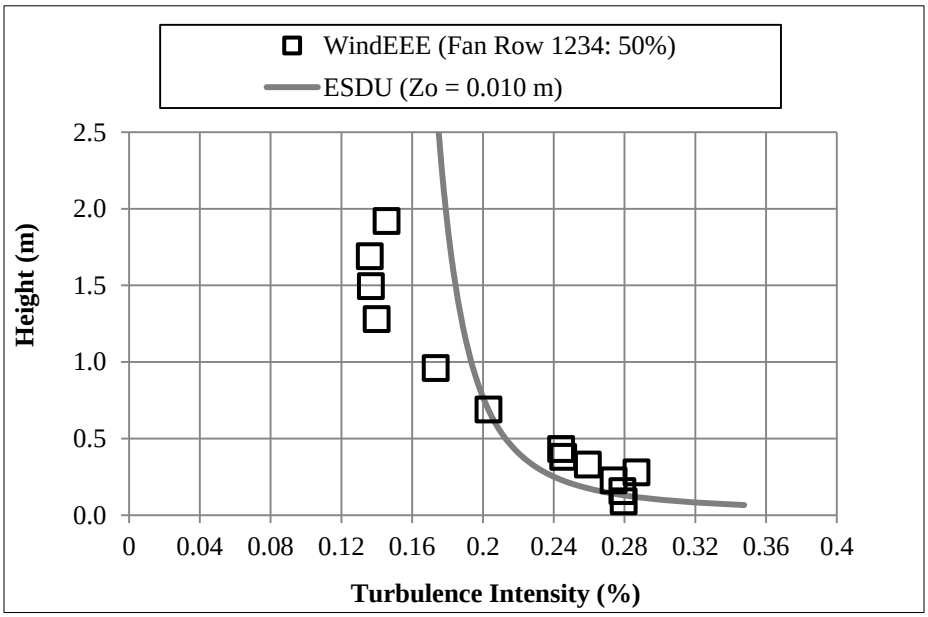

Figure 2.3: Comparison of mean turbulence intensity profile measured at WindEEE and ESDU standard for open terrain with Zo=0.01

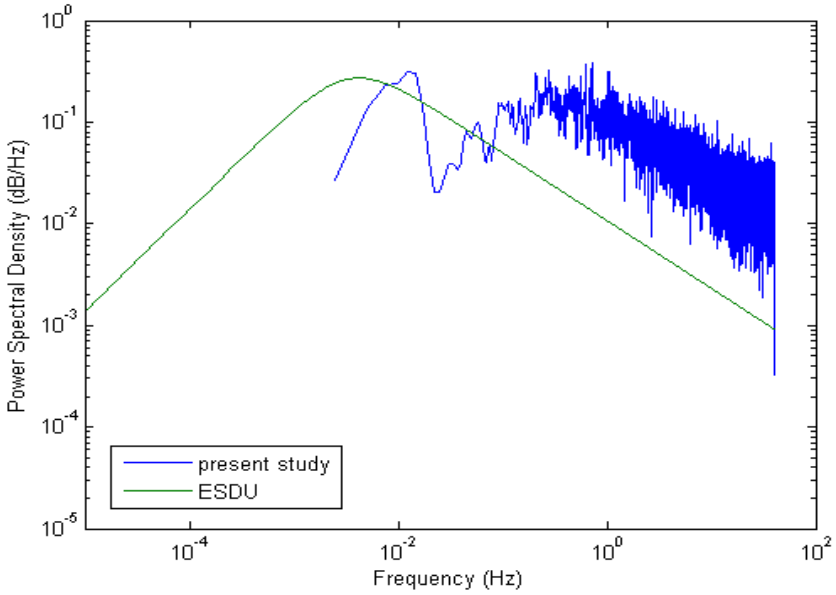

Figure 2.4: Comparison of spectra of stream-wise turbulence velocity measured at WindEEE and ESDU standard at the solar panel height, H=0.96 m

2.3 Experimental models

For conducting the experimental test, two types of test models are prepared. The first is a pressure test model which consisted of a supporting structure similar to the real solar panel, and a double layer clear sheet made of rigid Polycarbonate as a replacement of the real panel. This double layer sheet is employed to be instrumented with pressure taps, as shown in Figure 2.5. Each panel included 127 pressure taps with 1.5mm diameter on each side (508 taps in total) which recorded aerodynamic wind pressures on both sides of the model (lower and upper surfaces) during the tests. The total dimension of the model is 1960 mm×1990 mm with 12 mm gap between two layers which are placed in an aluminum frames and 20 mm gap between panel 1 and panel 2. This double layer panel is assembled on supporting structure of the actual solar panel at 25^{o} inclination. Figure 2.6 demonstrates the location of the first model on the turn table in the WindEEE.

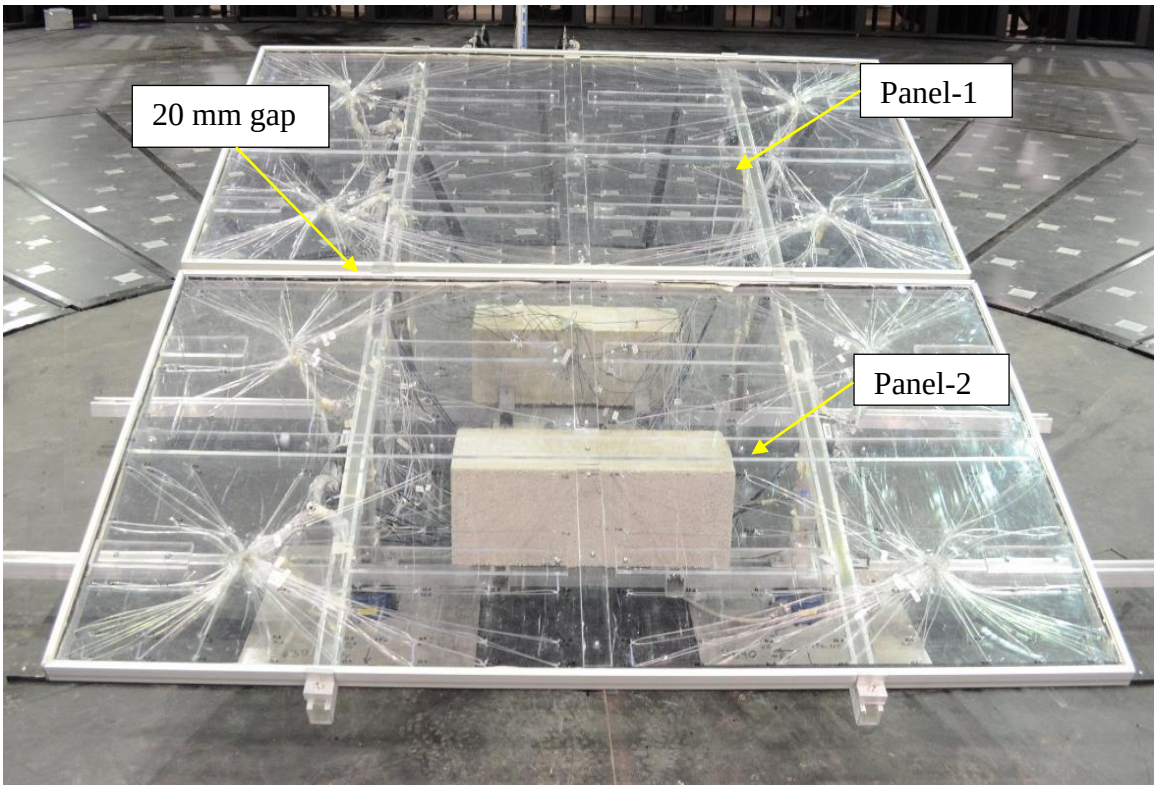

Figure 2.5: Pressure test model

Pressure taps are connected to the pressure data acquisition system through vinyl tubes. The tubes connectivity are described in detail in Section 2.6. Four circular holes with 50 mm diameter are provided on the lower surface of each panel as a way out for the tubes from the layers. The pressure taps layout on upper and lower sheets are displayed in Figure 2.7a and 2.7b.

The second test model is a full-scale solar panel fabricated with the same material and elements of a real solar panel (Figure 2.8), hence representing a full aero elastic model. This model consists of two individual panels placed at the top and bottom of the assembly with the same dimensions of the first model.

The inclination of the solar panels is set at 25° as typically used for southern Ontario latitude, for high energy product during summer seasons. Both models are mounted on three force balances in order to monitor their support reactions under a real wind loading profile. However, the real model is specifically employed to measure their support

reactions during the wind testing. The support reactions of the real models are recorded, for further structural analysis.

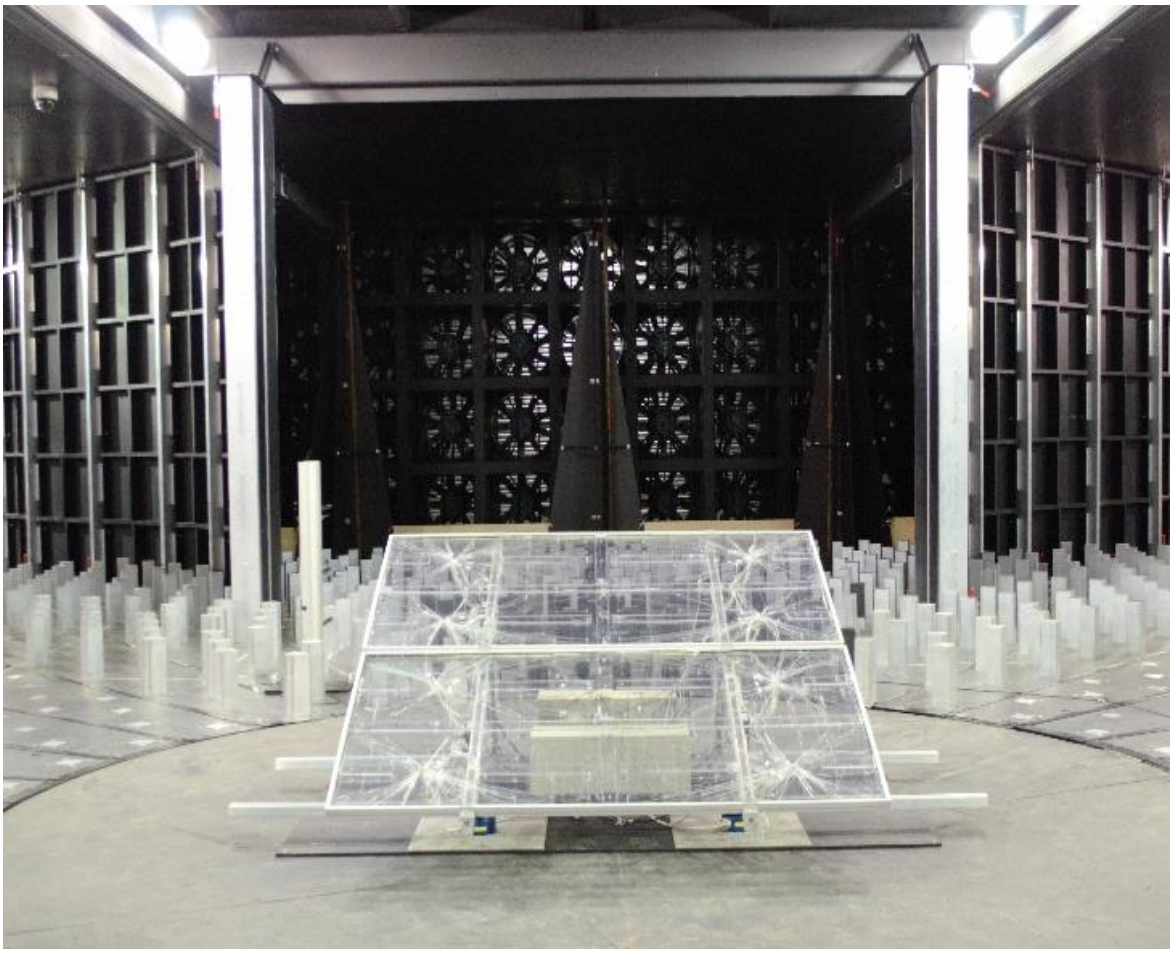

Figure 2.6: Pressure test model set-up in WindEEE

The wind pressure measurements are further used for Finite Element analysis conducted on supporting structure and the force-balance measurement is used to validate the FE model.

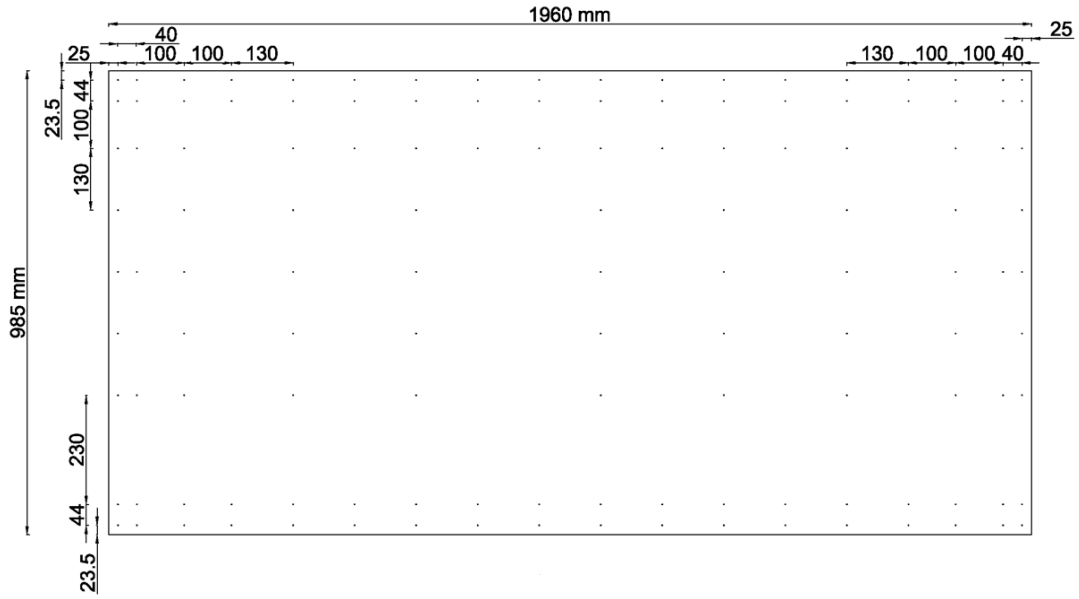

(a)

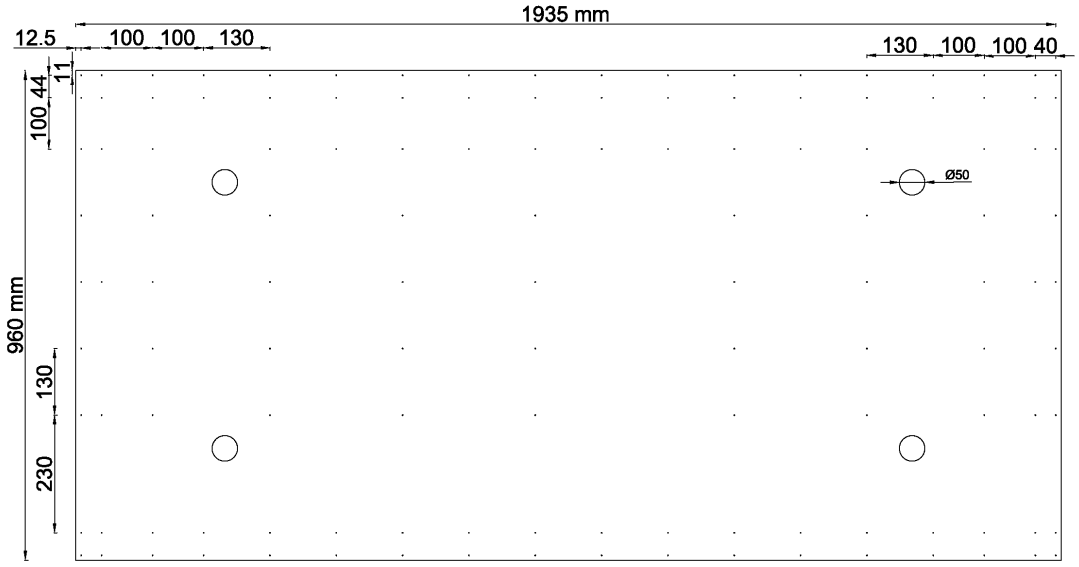

(b)

Figure 2.7: Tap layout of a panel (a) upper surface (b) lower surface (127 pressure taps on each)

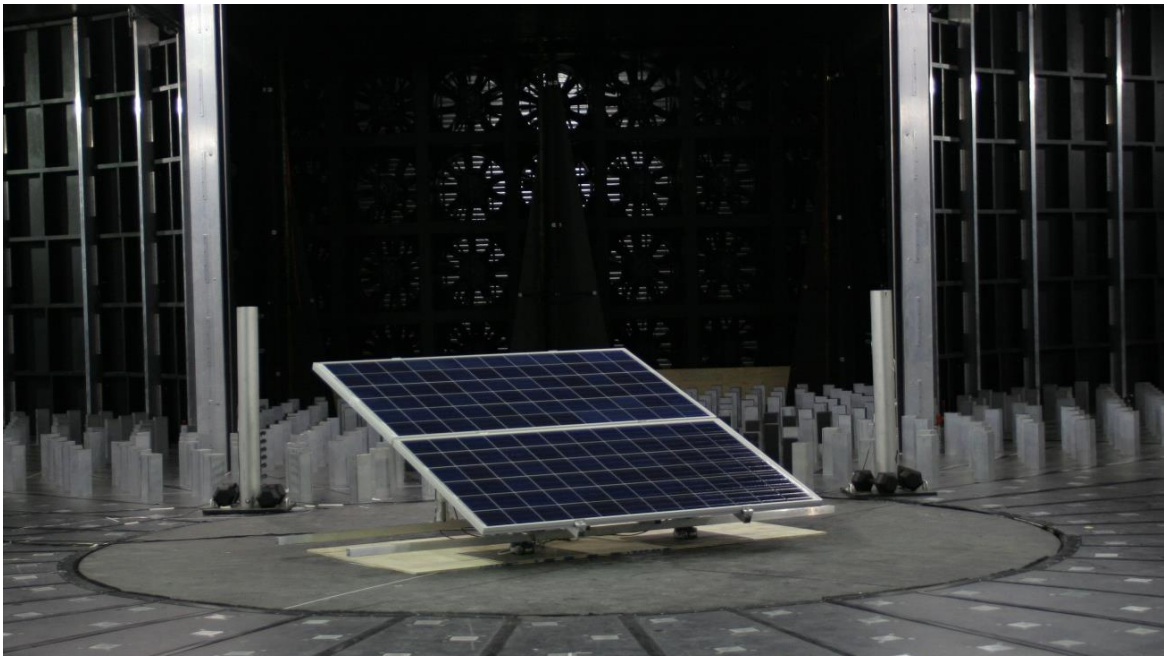

Figure 2.8: Aero-elastic model (full-scale solar panel) test set-up at WindEEE

2.4 Supporting structure of solar panel

The supporting structure of solar panel (solar Rack) is consisted of cold-form aluminum uni-strut sections which are bolted together with proprietary connections. The solar panel is placed in an aluminum frame which is clipped to the solar rack. Ground-mounted solar panels are usually connected together in a network consists of several rows and columns. The network of solar panels are usually stabilized using concrete ballast which adds to the weight of solar network and lead to higher stability. In a real network, two ballasts on each solar rack is placed. The same arrangement for a stand-alone solar panel using two concrete ballasts is used in the present study. The plan and elevation view of the solar rack as well the location of concrete ballast are shown in Figure 2.9. It is worth mentioning that the stability of a single solar panel is not the objective of this experimental work, as the stability it should be investigated in an entire network.

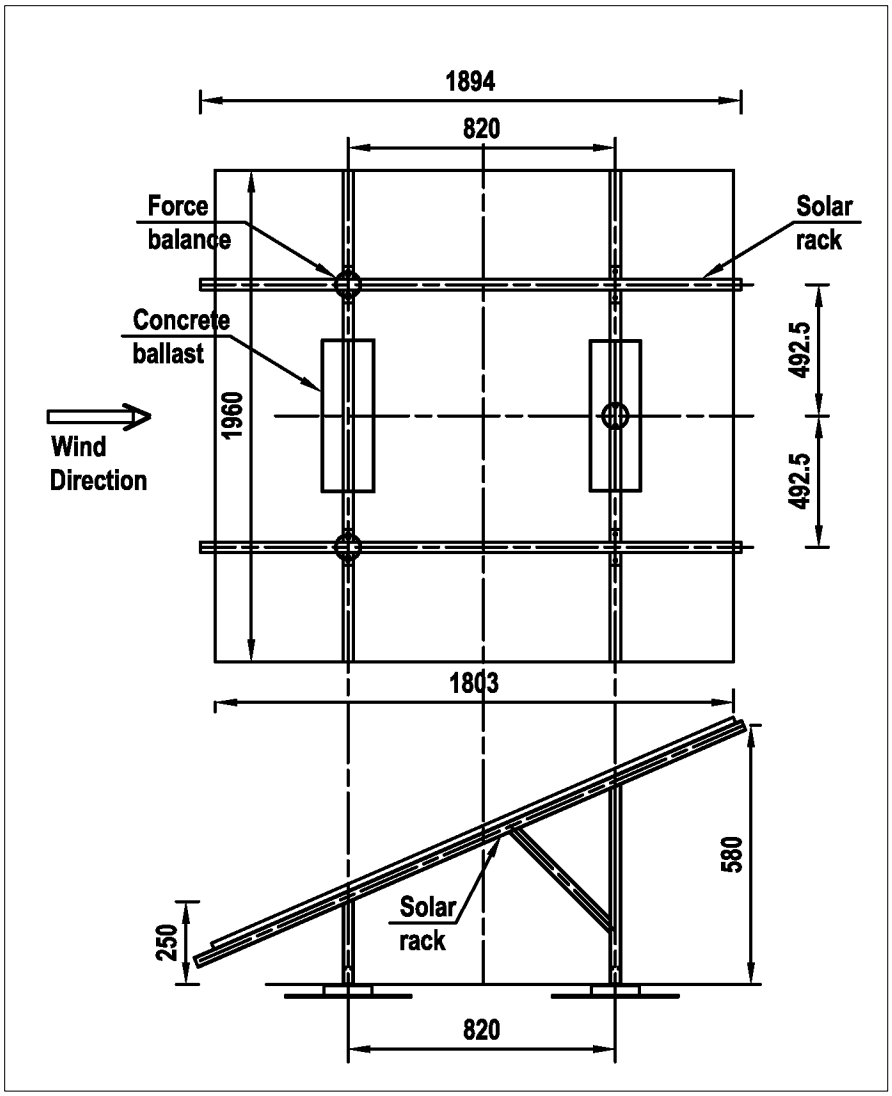

Figure 2.9: Solar panel supporting structure, concrete ballasts and location of force balances

2.5 Test arrangement in WindEEE

The schematic view of the entire plan of the test assembly is demonstrated in Figure 2.10. As shown in the figure, the model is placed on the turntable at the middle of the test chamber of WindEEE which could be adjusted for different wind angles of attack. A contraction with an area ratio of 36% is used to produce higher flow uniformity and to increase the base wind speed.

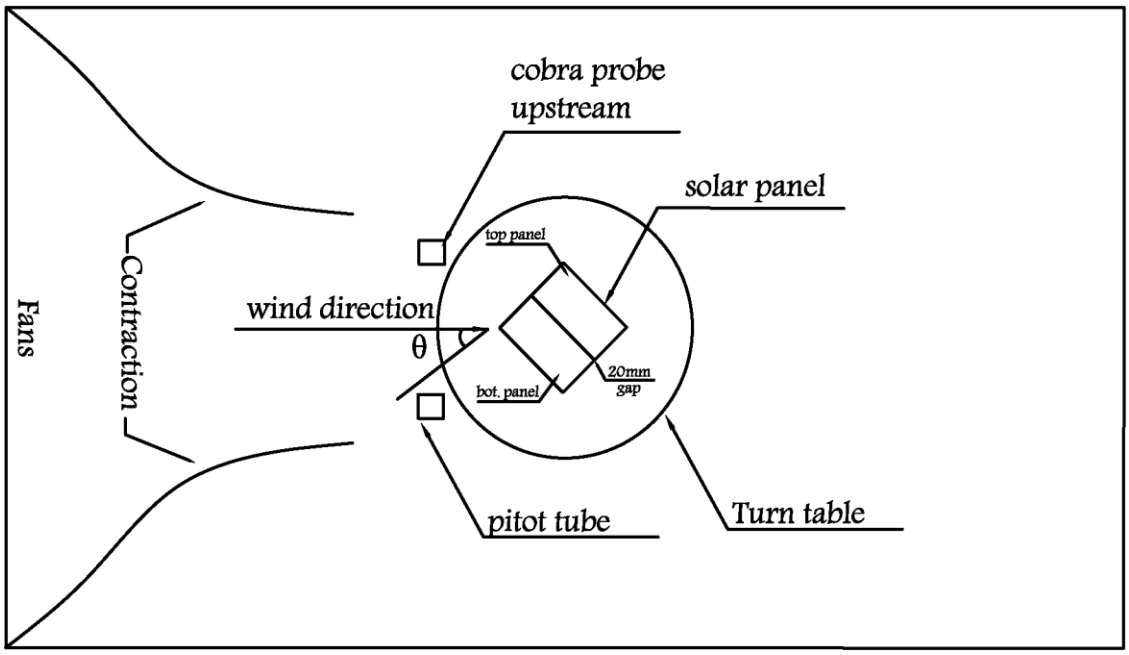

Figure 2.10: Schematic view of test setup in WindEEE

A pitot tube and a Cobra probe are utilized to measure the real-time velocity and pressure as shown in Figure 2.11. Pitot tube is typically used for wind experiments to measure the flow speed using differential pressure. Pitot tube is a slender tube with two holes; the front hole measures the total pressure and the side hole measures the static pressure. Using the difference between these pressures which is the dynamic pressure, pitot tubes calculates the flow velocity. Cobra Probe is a multi-hole pressure probe which is used to measure the velocity and local static pressure in real time. Cobra Probe operates in high frequencies and suites to measurement of turbulent flows.

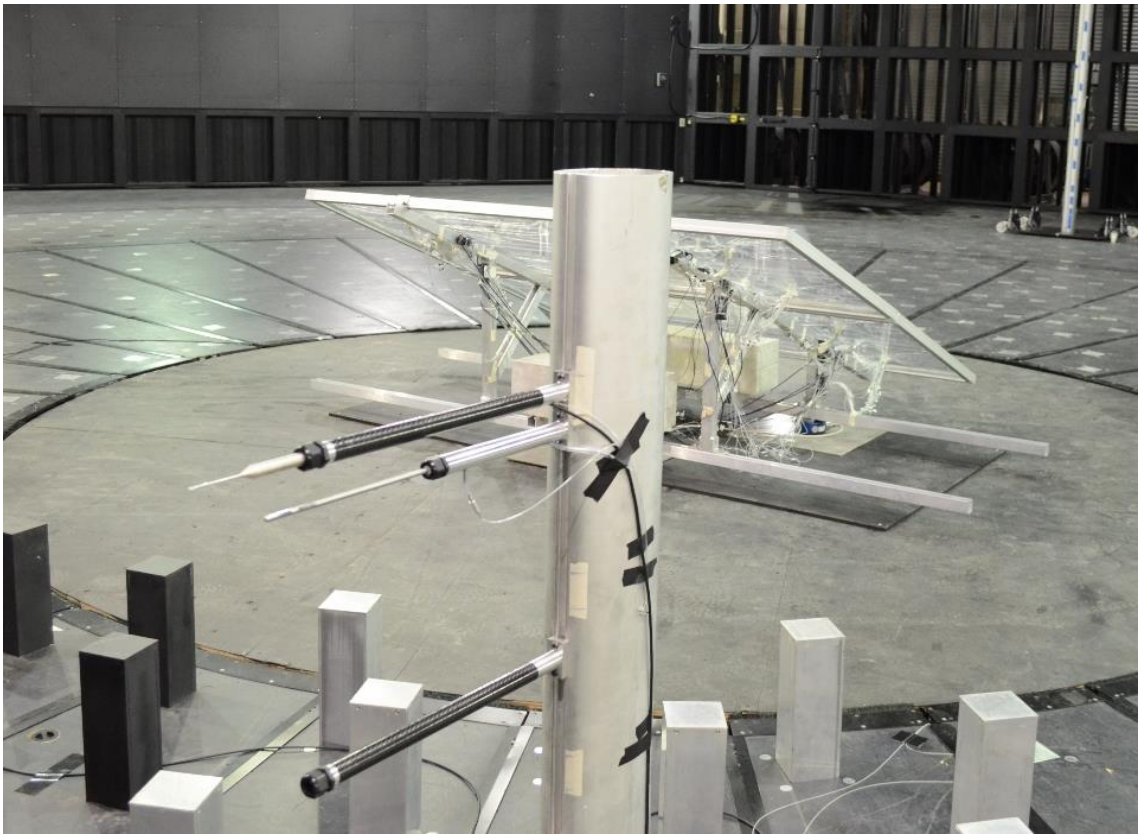

Figure 2.11: Cobra Probe and Pitot tube set-up in WindEEE

2.6 Instrumentation

The pressure taps of the solar panel model are connected to the data acquisition system through vinyl tubes with 1 mm diameter and 508 mm length. The tubes are clustered and pass through the holes of lower sheets. The other free side of the tube is attached to another tube with the same length and diameter through a brass restrictor in order to add more damping and reduce the response harmonics in the pressure instrumentation system (Figure 2.12). The tubes are ultimately connected to the scanners, as shown in Figure 2.13. For this study 16 scanners are required, each connected to 32 pressure taps (total number of 508 pressure taps) and the rest four ports of the scanners are connected to Pitot-tubes and cobra probe to measure the reference velocity. An attempt is made to attach all the tubes and the rack members to minimize their effect on the wind flow on the lower sheets during the experimentation.

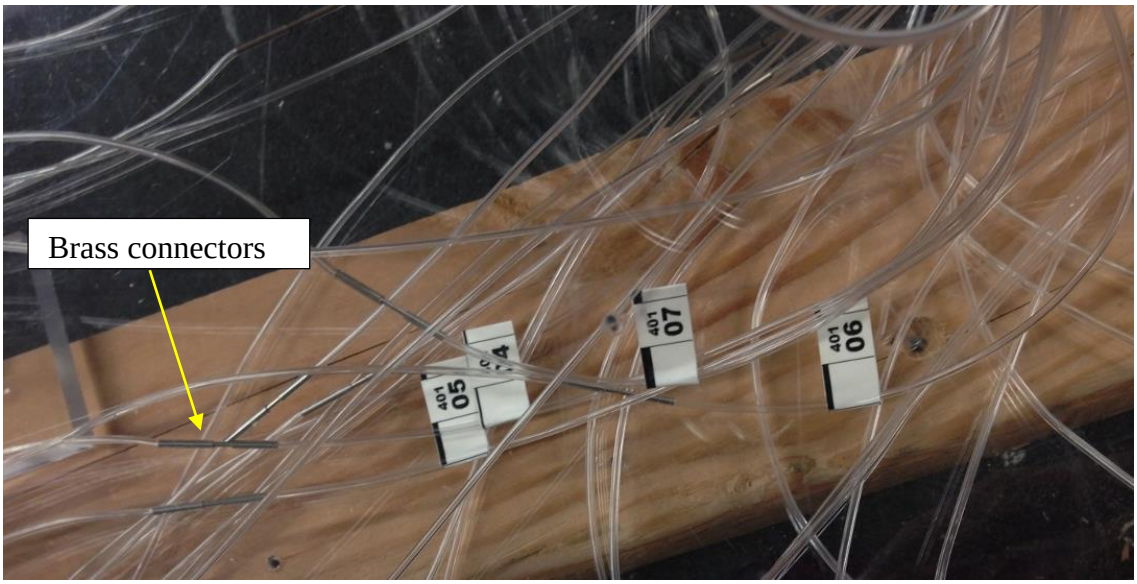

Figure 2.12: View of the connection of vinyl tubes using brass connectors

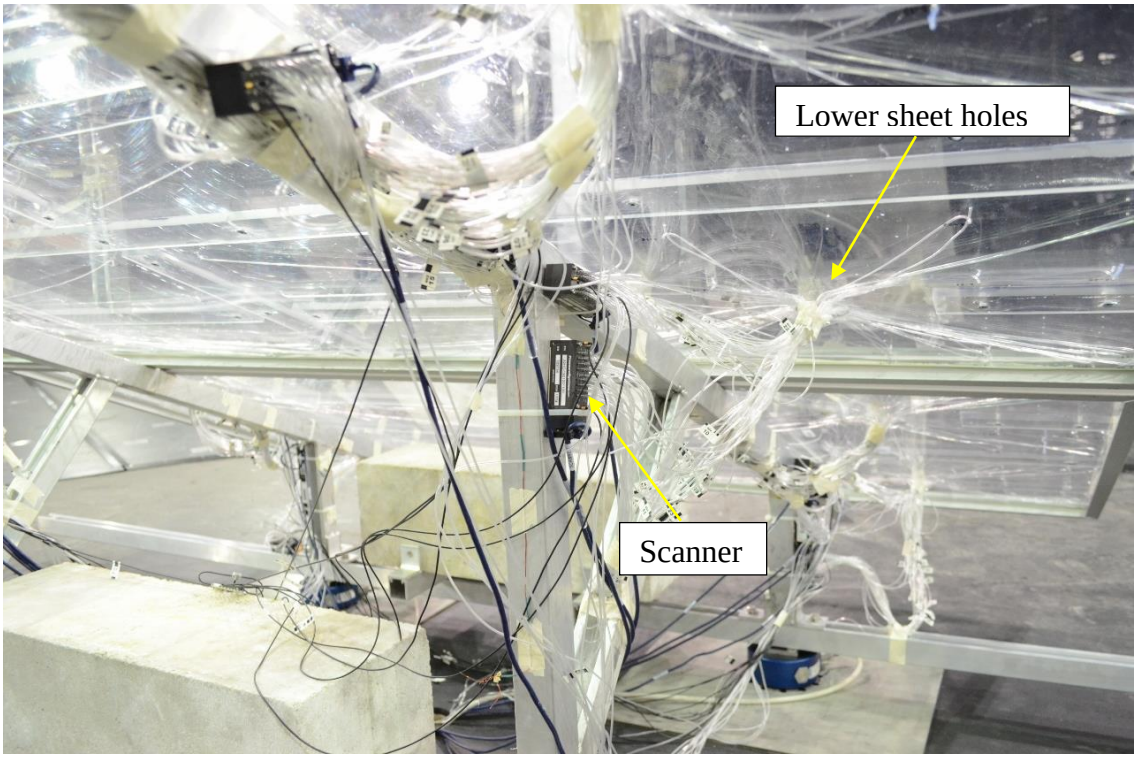

Figure 2.13: Bottom view of solar model showing the vinyl tubes and scanners

The scanners read the pressure time series at each tap, convert them to an electrical signal and transmit the signals to the WindEEE's computerized data acquisition (DAQ) system.

Each of the 16 scanners is connected to the DAQ (two Inithium M921001 (283) & M921002 (284)). The unit of recorded pressure data is an inch of water. The data is then converted to Pascal and transformed to pressure coefficients (Cp). The instrumentation and connection of the test set-up in the WindEEE is displayed in Figure 2.14.

Three force balances are installed under the solar racks to measure the wind induced base reactions. These instruments are connected to three different linear power supply box which are connected to JR3 (analog signal output). Then, the data are converted to NIDS (National Instruments Data acquisition System) through black DC (direct current) cables (Figure 2.14.). These force balances are capable measuring six components at the base of the racks: three force components in X, Y, and Z directions and three moment components about the X, Y, Z axes. It is initially clear that since the solar racks are truss-like frames and their supports are not rigid, the moment reactions are not considerable. The obtained forces and moments represent the overall loads transferred from the solar panels and its framing as well as the ballast. Throughout this study, however, the wind induced reactions are initially distinguished from the weight induced reactions for the sake of comparison of results.

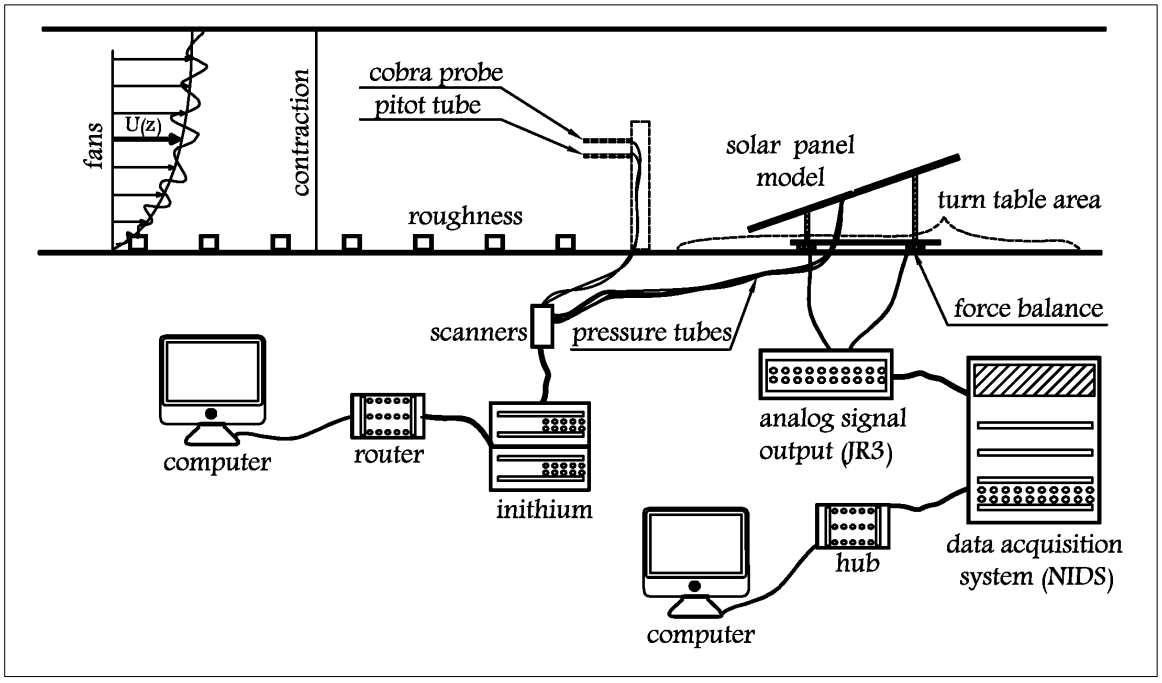

Figure 2.14: Instrumentation of the test set-up in WindEEE

2.7 Test procedure

The model is placed on a turntable and is connected to the WindEEE pressure DAQ system as described earlier. The solar panel model is subjected to uniform and boundary layer flow for open exposures and pressure data are recorded as summarized in Table 2.1. The real solar panel is tested for the same flows however, only their base reactions are recorded.

Table 2.1: The experimental test cases in WindEEE

Flow	panels	Angle of attack (θ)
Boundary layer flow	**Aero-elastic model**	0°, 10°, 20°, 30°, 40°, 45°, 50°, 60°, 70°, 80°, 90°, 100°, 110°, 120°, 130°,135°, 140°, 150°, 160°, 170°, 180°
Boundary layer flow	**Aerodynamic model**	0°, 10°, 20°, 30°, 40°, 45°, 50°, 60°, 70°, 80°, 90°, 100°, 110°, 120°, 130°,135°, 140°, 150°, 160°, 170°, 180°
Uniform flow	**Aerodynamic model**	0°, 30°, 45°, 135°, 150° and 180°

The duration of each test and data recording is three minutes, which is statistically-long enough to obtain an accurate mean pressure. The pressure is measured at the frequency value of 600 Hz. The tests are carried out for 21 wind angles at 10-degree intervals from 0° to180° in addition to 45° and 135°. However, the results from many of the oblique wind angles (e.g. 10, 20, 30, and 40 and corresponding angles in other quarters) are not discussed in detail in this study, as they are found to be non-critical.

The blockage ratio recorded at the WindEEE was 3%, which is less than the minimum value recommended in ASCE-7 equal to 8% [ASCE 2010]. Table 2.2 summarizes some characteristic of the pressure test.

Pressures are measured with respect to the mean static pressure at the WindEEE test section, corresponding to the mean static pressure in the full-scale wind flow. At the location of each pressure tap, the time history of the pressure coefficient, $C_p(t)$, is obtained from the time history of the instantaneous surface pressure, p(t), as follows:

$$\mathrm{Cp(t)} = \frac{\mathrm{p(t)} - \mathrm{p_{static}(t)}}{\frac{1}{2}\rho \mathrm{U}^2} \qquad (2.1)$$

where ρ is the air density at the time of the test, and U is the mean wind speed measured at the mean height of the solar panel over the entire test duration.

Table 2.2: Characteristic of the pressure test

Scale	Blockage at WindEEE [%]	Record length of each test [s]	Sampling rate [Hz]
full-scale	3%	180	600

The net pressure on each tap is evaluated through the difference between pressures on the two corresponding taps on both sides of the solar panel. The net pressure coefficient at each tap, $Cp_{net}(t)$, is the simultaneous difference between the pressure coefficient at the upper surface, $Cp_{upper}(t)$, and the corresponding pressure coefficient at the lower surface, $Cp_{lower}(t)$, at the same location (Equation 2.2).

$$Cp_{net}(t) = Cp_{upper}(t) - Cp_{lower}(t) \quad (2.2)$$

The obtained results of pressure tap and force balances are discussed and analyzed in detail in Chapter 3.

Chapter 3

3 Aerodynamic data analysis and discussion

This chapter outlines the results and discussion of the wind testing conducted on solar panel models. The pressure contours for different wind profiles and various wind angles of attack are presented. The accuracy of different pressure tap layouts and resolutions are investigated and the Reynolds number for the wind profile is discussed. The base reactions that calculated from the force balances are compared with those obtained from the pressure taps. Finally, critical wind directions are recognized and several conclusions are made. Results of comparative analyses with other studies are discussed and conclusions are summarized.

3.1 Surface pressure distribution

The mean and net pressure coefficient contour plots for upper and lower panels are displayed in Figure 3.1 for four wind angles of attack of 0^o, 45^o, 135^o and 180^o. The results are obtained for boundary layer wind profile with 50% of the fan speed (mean reference velocity of 56.2 km/h) and a roughness value of 0.01. The results for the critical wind angles of attack are presented in the following sections.

3.1.1 Head on, forward wind angle of attack (0^o)

The pressure distribution on the model at 0^o wind angle of attack is almost symmetric about the center line of the panel. The contour plot also reveals that the positive magnitude of the pressure coefficients is largest at the leading edge where the flow first impacts the model. As the flow passes over the panel towards the trailing edge the pressure drops. Shademan et al. (2010) previously identified the same pressure distribution and critical locations at 0^o wind angle of attack for a similar inclination of solar panel in a CFD simulation. There is a little variation between the two panels as a result of the gap presence. The 20 mm gap between the panels induces an abrupt change in pressure distribution in the direction of the flow, as the wind flow can pass through the gap.

Wind AOA	Net mean Cp	Upper surface Cp mean	Lower surface Cp mean
0 degree	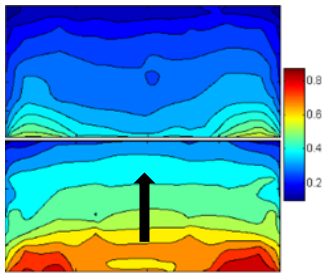	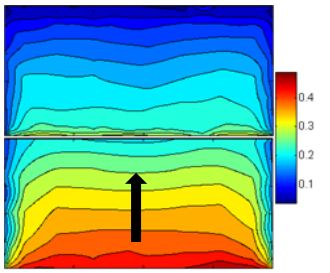	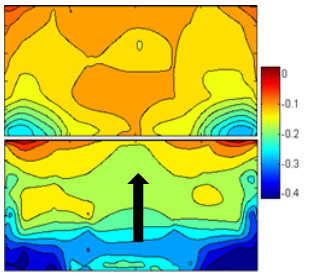
45 degree	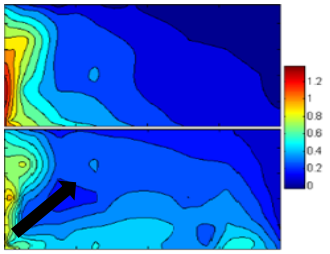	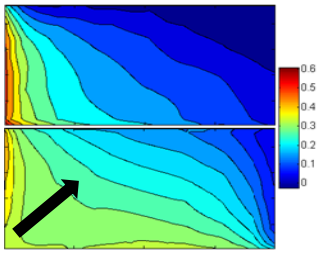	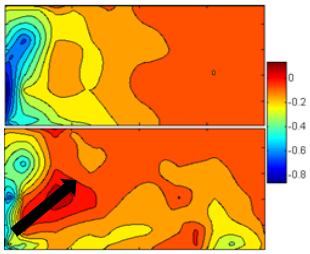
135 degree	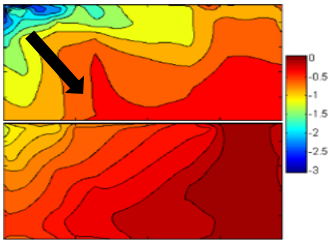	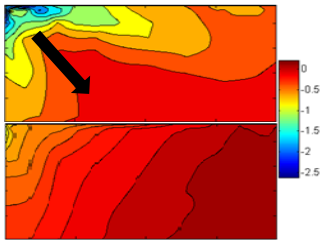	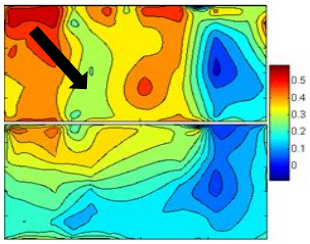
180 degree	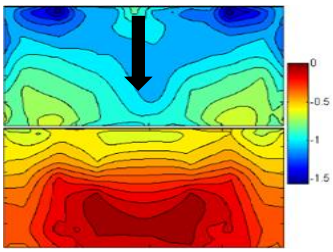	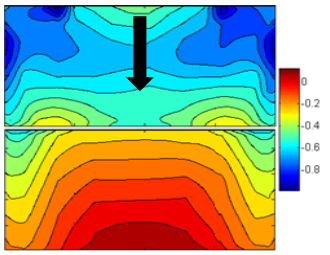	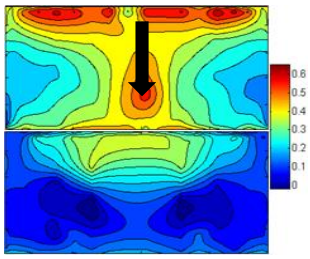

Figure 3.1: Mean and net pressure coefficient (Cp) contours on the panels for different wind angles of attack

3.1.2 Head on, reverse wind angle of attack (180^o)

The contour plots of net pressure coefficient show that the panel is critically loaded when the wind angle of attack is head-on at 180^o wind angle of attack. When the flow approaches the solar panel in the reverse direction, i.e. 180^o wind angle of attack, the lower surface faces the approaching wind while the upper surface lies in the wake of the wind flow. The pressure distribution on the lower surface, which now faces the oncoming wind, is also symmetric across the mid plane. As the upper surface pressure is subtracted from lower surface pressure, the mean net pressure is a negative value across two panels as shown in Figure 3.1.

3.1.3 Oblique wind angles of attack (45^o and 135^o)

When the wind approaches the model at angles other than 0^o and 180^o, there is no symmetry of the pressure distribution across the panel, as displayed in contour plot of Figure 3.1. The asymmetric pressure distribution pattern is also obtained for other oblique angles from 10^o to 170^o. Figure 3.1 demonstrate that mean Cp values decrease diagonally on the surfaces of panels along the wind angle of attack. This is expected as the flow accelerates at the leading edges or corners and creates a low pressure region on the panel surface and gradually decrease in the flow direction, forming a horseshoe vortex.

Mean Cp distributions of oblique angles illustrate a separated region for both 45^o and 135^o wind angles of attack which confirms possible existence of corner vortices. Formation of the separated region and corner vortices are more pronounced on panel-1 (top panel) while a mean Cp of the panel-2 show almost a modest uniform distribution. For 45^o and 135^o wind angles of attack, the asymmetric pressure distribution and corner vortices are also reported in previous studies (Jubayer 2014, Abiola-Ogedengbe 2013).

3.2 Pressure equivalent

For the design and stability control of the solar racks, the total wind force on the panels is required, which is obtained by integrating the pressure on the panel surface with the corresponding tributary area. This pressure integration is given by Equation 3.1 which is the summation of pressure multiplied by its tributary area at each tap.

$$F_t = \sum_{i=1}^{n} p_{net,i} \times A_i \tag{3.1}$$

where F_t is total force applied on panel, $p_{net,i}$ represents the net pressure on tributary area of the tap number "i", and A_i is the tributary area of the tap number "i".

The equivalent pressure (P_{eq}) is evaluated as the total force divided by the total area of the panels using Equation 3.2. The physical meaning of P_{eq} is that if a uniform pressure with the value of P_{eq} is applied on the surface of a solar panel, it creates the same magnitude of force as the original pressure. By implementing P_{eq}, the variation of the applied load on the panels can be easily illustrated in different wind angles of attack as shown in Figure A.1 in appendix A. Which P_{eq} is usually expressed in terms of a dimensionless wind pressure parameter that is referred as equivalent pressure coefficient ($C_{Peq.}$) and is defined as Equation 3.3.

$$P_{eq} = \frac{\sum_{i=1}^{n} p_{net,i} \times A_i}{\sum_{i=1}^{n} A_i} \tag{3.2}$$

$$Cp_{eq} = \frac{\sum_{i=1}^{n} Cp_{net,i} \times A_i}{\sum_{i=1}^{n} A_i} \tag{3.3}$$

where V_o is reference velocity equal to 15.88 m/s. Figure 3.2a, 3.2b and 3.2c represent mean, maximum and the minimum equivalent pressure coefficient on panels, respectively, obtained from the time history of the pressure taps. The maximum and minimum values are obtained statistically by using the method of Gumbel distribution assuming the probability of non-exceedance of 95%. Figure 3.2a shows that the maximum force occurs between 160^o and 180^o wind angle of attack, while Figure 3.2c confirms that the maximum force occurs at 180^o wind angle of attack. So the stability of the solar panel should be controlled in the most critical direction which is the transverse drag force (180^o). Figure 3.2b shows that the maximum positive drag force occurs at 0^o.

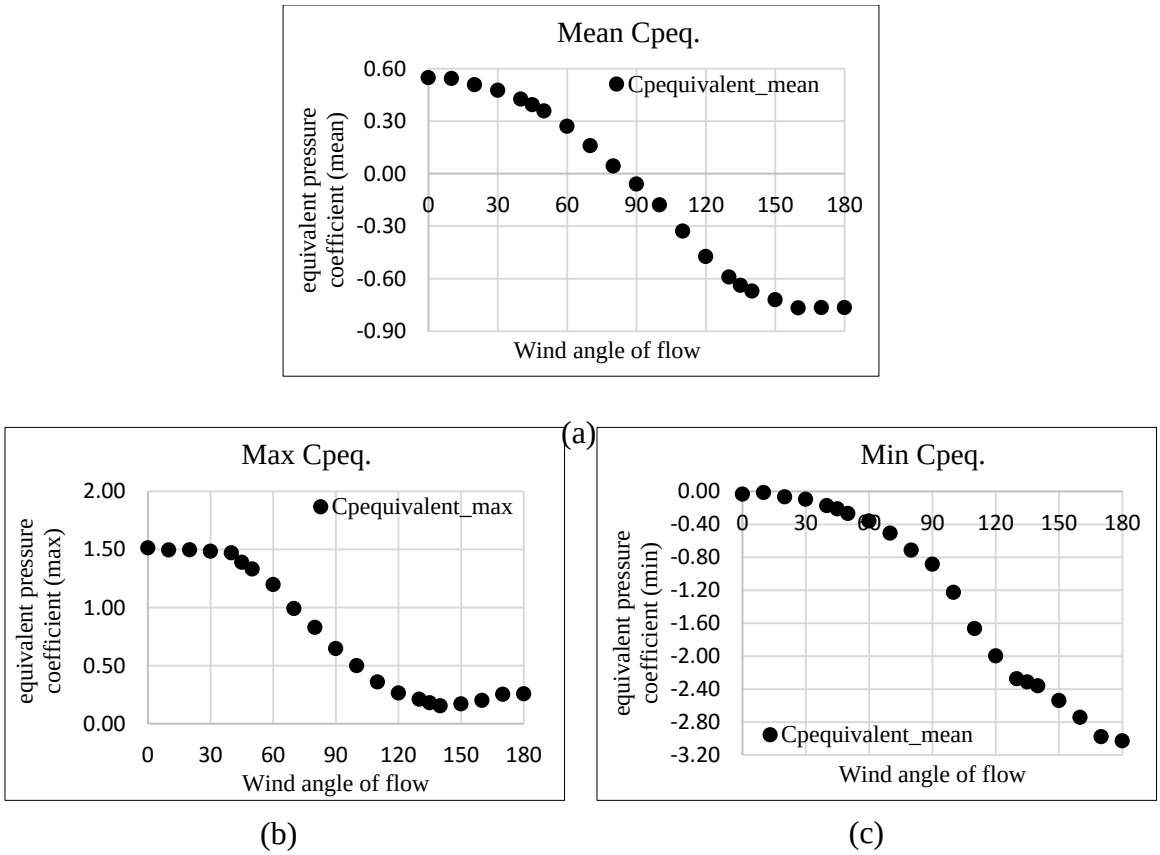

Figure 3.2: (a) Mean, (b) maximum and (c) minimum equivalent pressure coefficient for all wind angles of attack

3.3 Pressure coefficient comparison with literature

The pressure coefficients on the full-scale solar panel model of the present study are compared with the results of the 1:10 scaled experiment conducted by Aly and Bitsuamlak (2013) in the Boundary Layer Wind Tunnel Laboratory. This comparison is carried out for similar inclination angle of the panel (25^o) and wind angle of attack of 0^o and illustrated in Figure 3.3. It is to be noted that the solar panel tested by Aly and Bitsuamlak (2013) is longer 9200 mm×1400 mm compared to the present solar panel which is 1960 mm×1990 mm. Figure 3.3 shows that the pattern of the net pressure coefficient of the scaled solar panel model is in agreement with the full scale solar panel model obtained in this study.

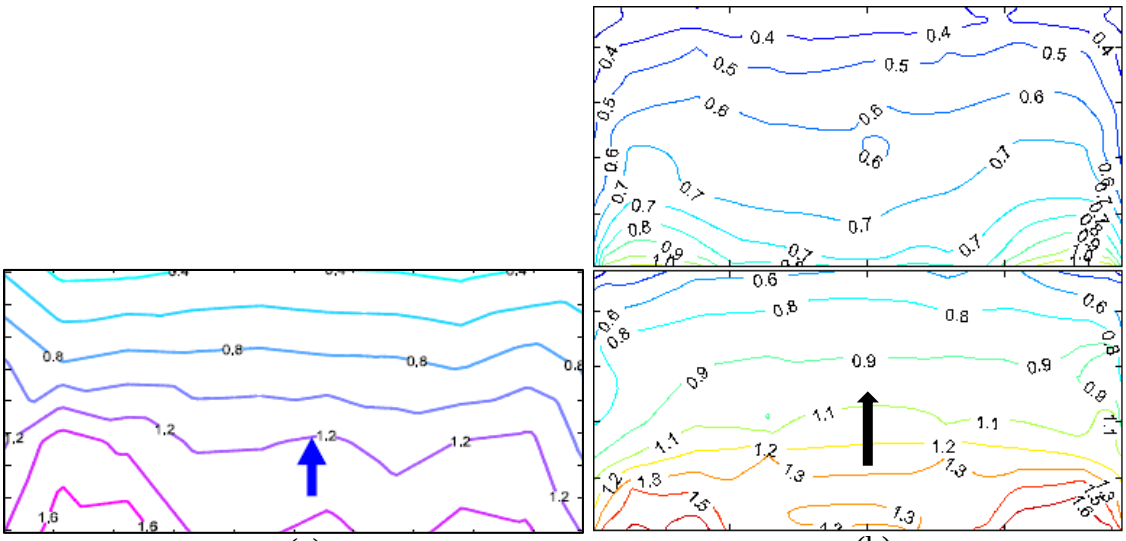

Figure 3.3: Comparison of mean net pressure coefficient of solar panel with 25º slope, a) 1:10 scale (Aly et al. 2012), b) full-scale model

Another comparison analysis is carried out with the aerodynamic results presented in Abiola-Ogedengbe et al. (2015). Figure 3.4 shows the model configuration for the two studies. Abiola-Ogedengbe et al. (2015) investigated an experimental model of a single panel at 1:10 scale (with 25º inclination) in the Wind Tunnel I at the University of Western Ontario. Figures 3.5 and 3.6 compare the mean C_p values along the mid-line of the panel for 0º and 180º wind angles of attack in both studies, respectively. To make the comparison meaningful, reference pressure and wind speed for calculation of Cp are taken at the same location. For the sake of comparison, the results are also normalized to the unit width of the panel to avoid the effect of different geometries.

A fairly good match is observed between C_p of the upper panel of both studies in 0º and 180º, however, there is an abrupt change in the present study graphs at the middle of flow path (50% b/B) which can be attributed to the presence of 20 mm gap between panel-1 and panel-2.

The graphs of the mid-line C_p of the lower surface of the panels are not in an agreement as good as the upper surface. This difference in pressure on the lower surface of the solar panel is attributed to the presence of the large concrete ballasts in the full-scale assembly which will alter flow condition on the lower surface of the solar panel. This can be clearly

seen in graphs of Figure 3.6 where b/B=1. The pressure tubes coming out from the lower surface of the solar panel may have contributed, but it is very significant compared to the concrete ballast. The 1:10 scaled model of Abiola-Ogedengbe et al. (2015) pulled the pressure tubes from side edges which created good condition for 0^0 and 180^0 wind angle of attack. However, this arrangement cannot be used for the oblique wind angles of attack. Despite the justifiable differences in the lower surface of solar panels and that of the effect of the gap, the magnitude and the variations of the Cps over the solar panels show good agreement between the two studies carried out at different scales. This confirms the conclusion made by Aly and Bitsuamlak (2014) stating that within the geometric scale of 1:10 to 1:50, mean wind loads on the solar panels are independent of the model scale (Aly and Bitsuamlak 2013).

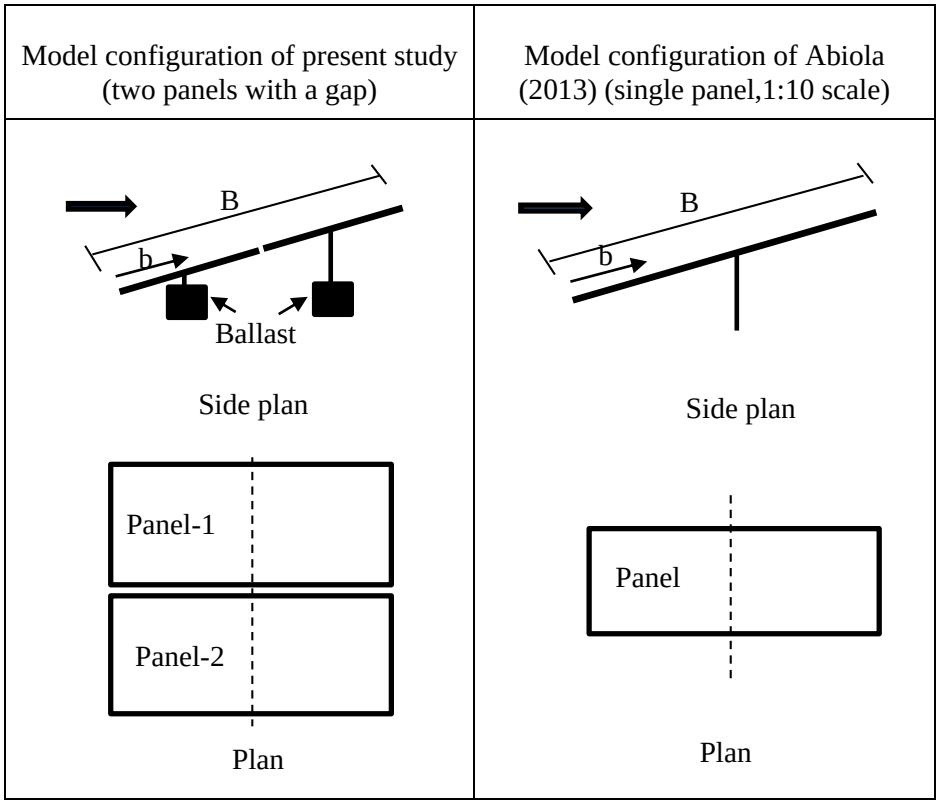

Figure 3.4: Model configuration of present study and Abiola-Ogedengbe (2013) with 25º inclined panel at 0º wind angle of attack

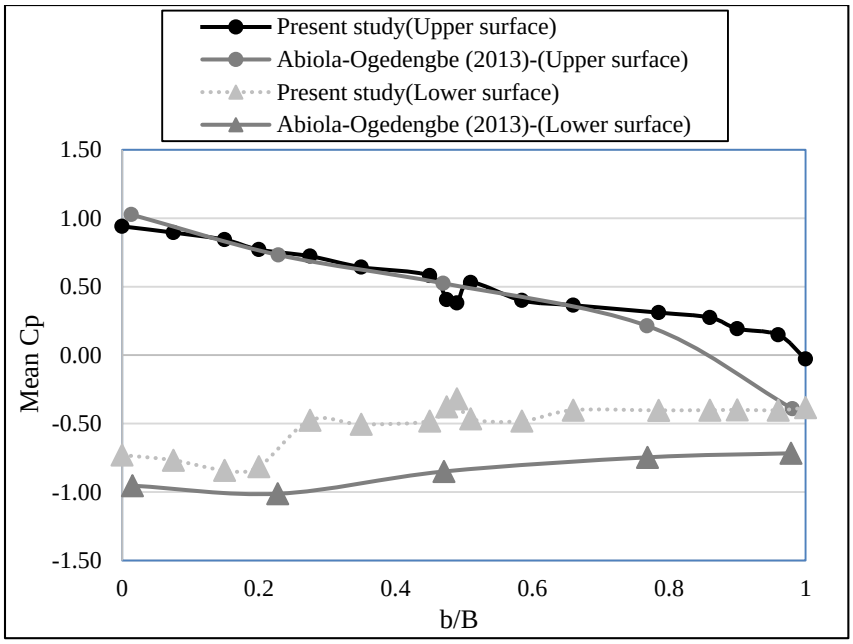

Figure 3.5: Mean Cp profiles along the mid-line of the panel surface for wind angles of attack of 0º

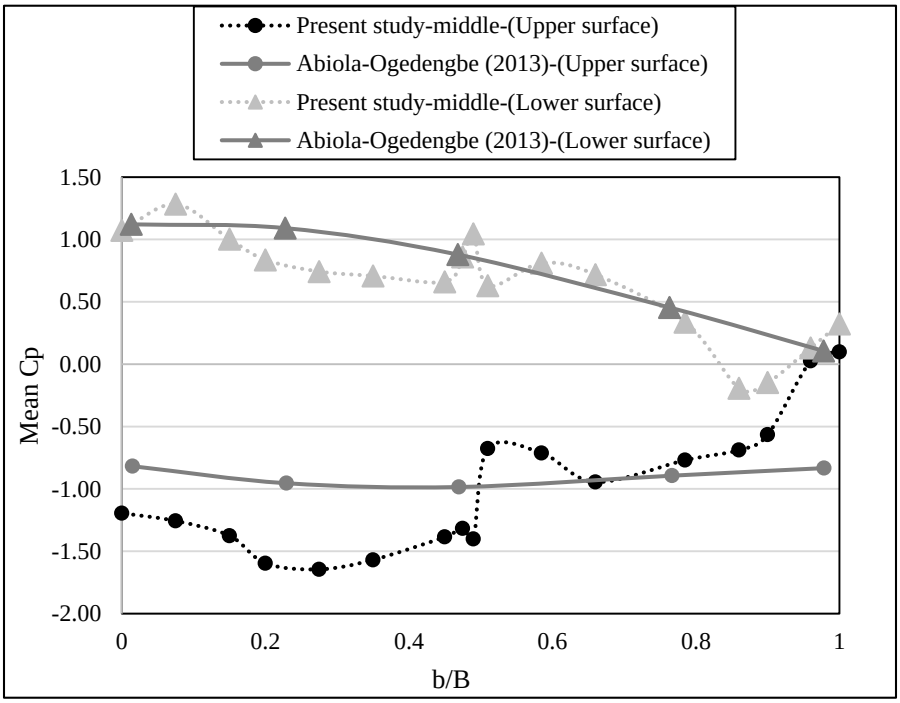

Figure 3.6: Mean Cp profiles along the mid-line of the panel surface for wind angles of attack of 180º Figure

3.4 Effect of pressure tap resolutions

One of the common challenge, while testing small structures (such as solar panel, roof pavers etc.) in the traditional boundary layer wind tunnel is their small size, limiting the number of taps that can be installed (Aly and Bitsuamlak 2013, Aly and Bitsuamlak 2012, Asghary et al. 2014) . The present study, owing to its large size, allows to study the effect of tap resolution on the overall wind loading and the ability to capture local pressure distribution. In the present study, wind pressure on the solar panel model is measured through 254 pressure taps incorporated in each of lower and upper sheet of the panel (total number of taps 508). The number of the taps divided by the area of the panel can describe the tap resolution. Incorporating higher density of pressure taps (hence higher resolution) clearly helps to accurately measure the pressure distribution.

A comparative study is carried out to evaluate the effect of arrangement and resolution of the pressure taps. Figure 3.7 shows the four resolutions that are considered in the present comparison. The 508 tap usage is referred as R100 to represent Resolution of 100% taps used (i.e. high resolution). Some of the taps are eliminated from the analysis to create less resolution tap layouts. Accordingly, the following tap resolutions are created: R32%, R16% with mid taps (layout-3) and R16% with edge taps (layout-4) as shown in Figure 3.7. The full tap layout (R 100%) is selected as a benchmark to evaluate the low resolution tap layouts which are in fact comparable to those used in the traditional boundary layer wind tunnels.

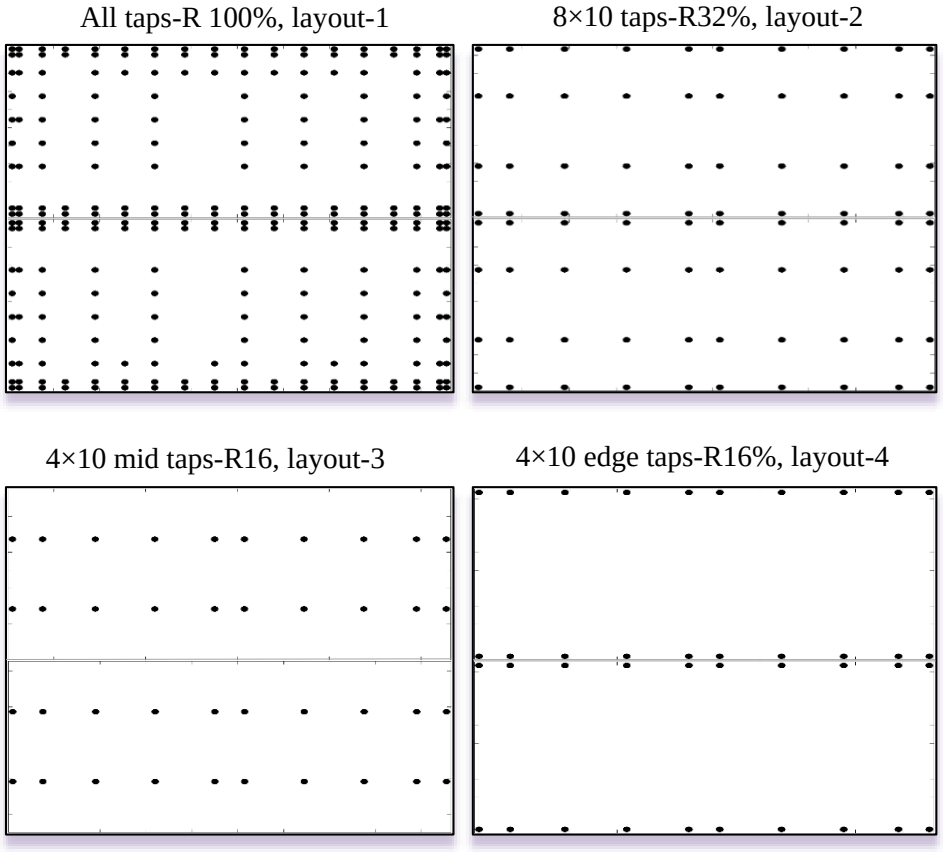

Figure 3.7: Pressure tap layout for four different resolutions

The mean net pressure coefficient contours for each tap resolution are plotted for 0, 45, 135 and 180 degree wind angles of attack as shown in Figures 3.8, 3.10, 3.12 and 3.14, respectively. The equivalent minimum, maximum and mean net pressure coefficients (Cp_{min}, Cp_{max} and Cp_{mean}) are also evaluated for each case and plotted in Figures 3.9, 3.11, 3.13 and 3.15. The peak and mean equivalent net pressure coefficients (Cp_{min}, Cp_{max} and Cp_{mean}) are evaluated following a similar procedure discussed for equivalent pressure (see Equation 3.2).

The following observations are made from comparisons shown in Figures 3.8 to 3.15:

- It appears that a high density resolution is required to capture all the aerodynamic features of pressure on the solar panel surfaces. However, layout-2 (R32%) in all cases, fairly represents the pressure distribution without compromising the

accuracy of the peak values. This means that the pressure contour and equivalent pressure coefficients obtained by R32% are reasonably acceptable and close to high resolution tap layout (R100%).

- Comparison of layout-3 (R16% with mid taps) and layout-4 (R16% with edge taps) indicates the fact that the edge taps are more influential in better representation of contour plots, as the contour plots of the layout-4 in all wind angles of attack are more similar to the higher resolution tap layout, compared to layout-3. However, the values of equivalent pressure obtained for layout-4 are the least accurate with respect to layout-1 (R100%). Conversely, layout-3 provides a better estimation of equivalent pressure coefficient in comparison with layout-4 however, demonstrates the least accurate contour plots.

- Comparison of the bar graphs in all cases indicates that the mean pressure is almost insensitive to the resolution percentage. However, peak pressure coefficients (Cp_{min} and Cp_{max}) significantly vary with resolution change. The peak pressure coefficients for less density layouts, e.g. layout-3 and layout-4, are inaccurate and not reliable. We can also conclude that the mean pressure solely, is not adequate to determine the effective resolution percentage.

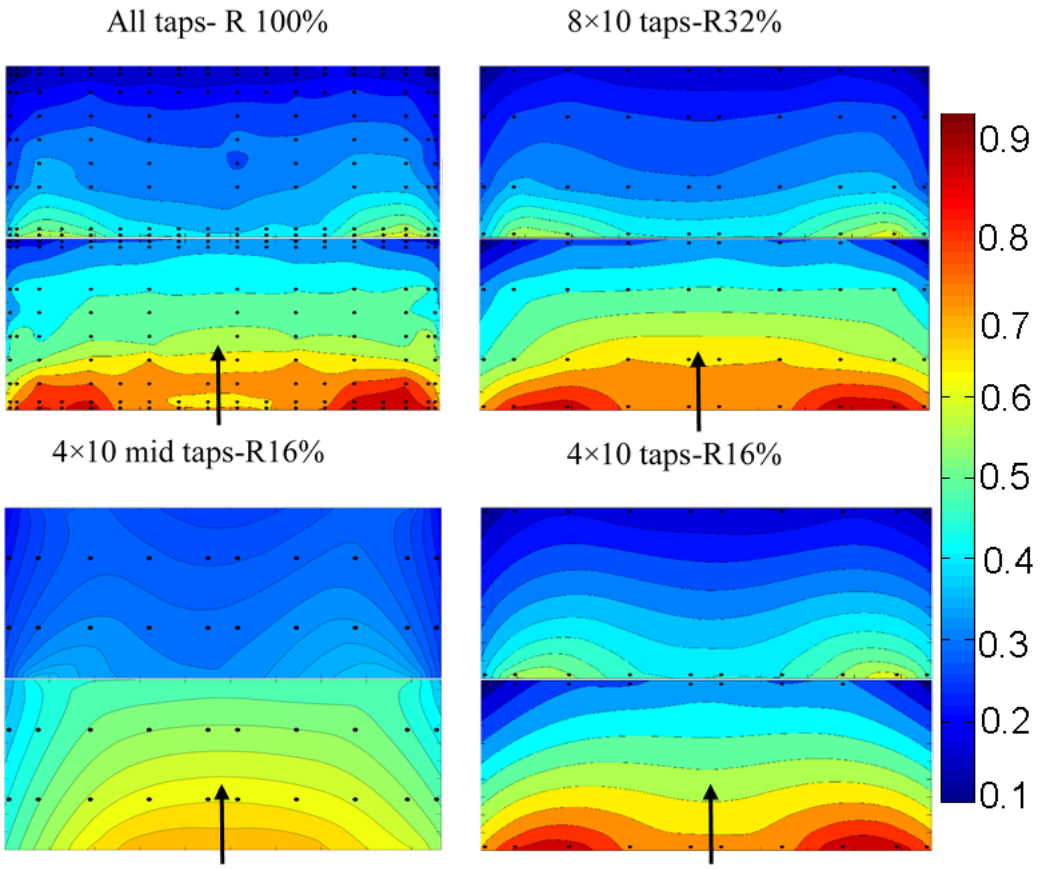

Figure 3.8: Net mean pressure coefficient (C_p) distribution of 0 degree wind angle of attack for different resolution

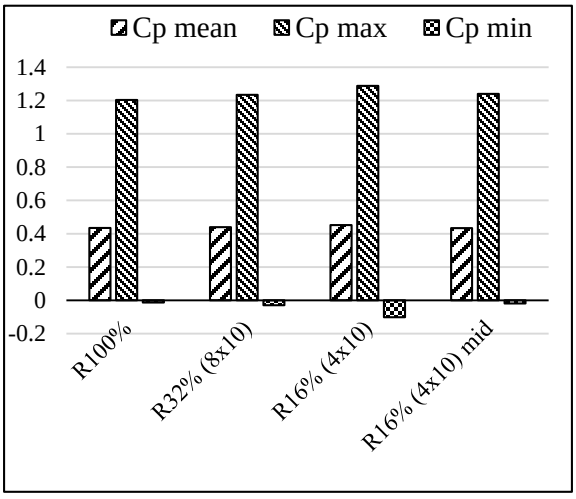

Figure 3.9: C_{Pnet} of different pressure tap layouts at 0 degree wind angle of attack

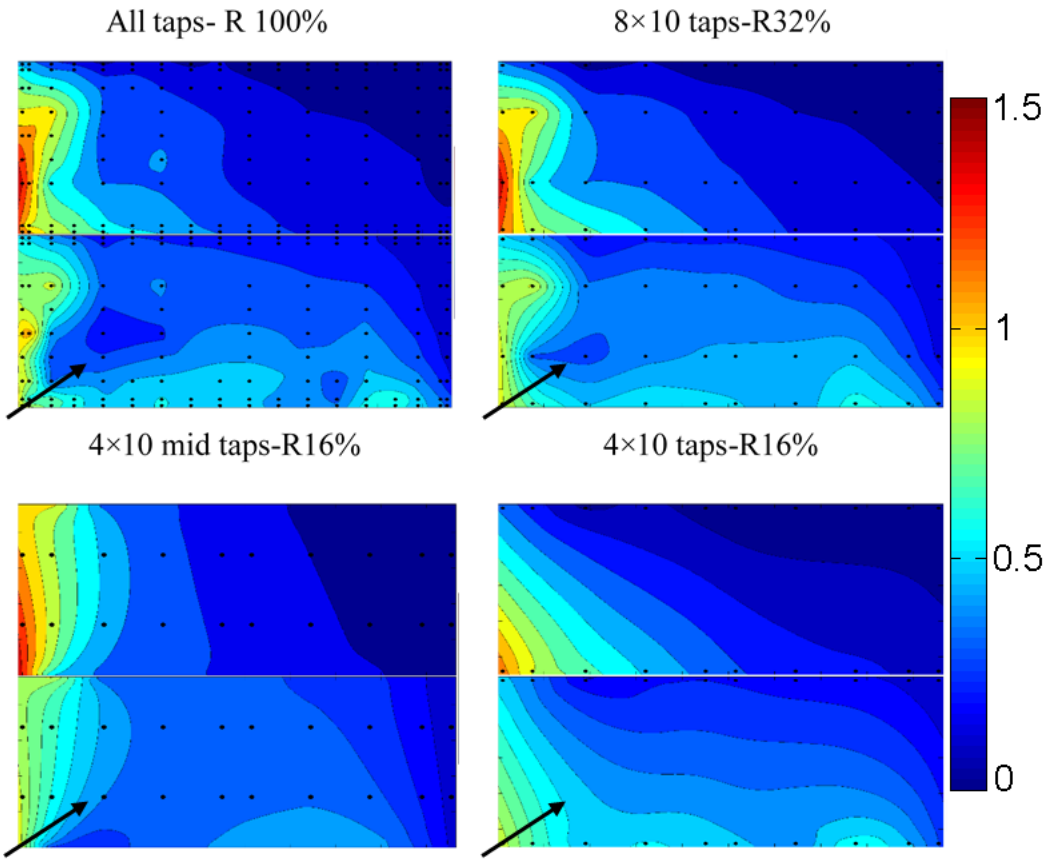

Figure 3.10: Net mean pressure coefficient (C_p) distribution of 45 degree wind angle of attack for different resolution

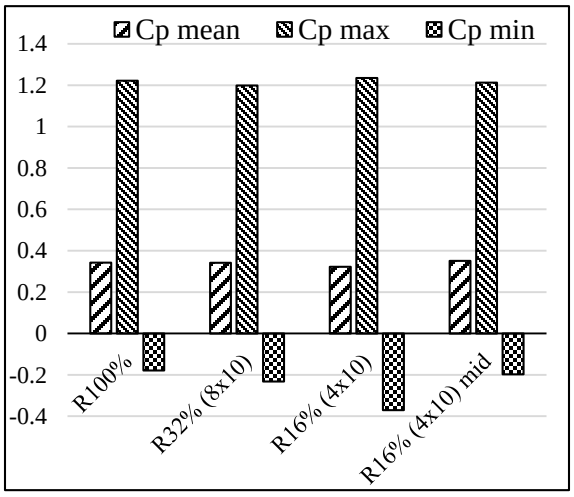

Figure 3.11: CPnet of different pressure tap layout for 45 degree wind angle of attack

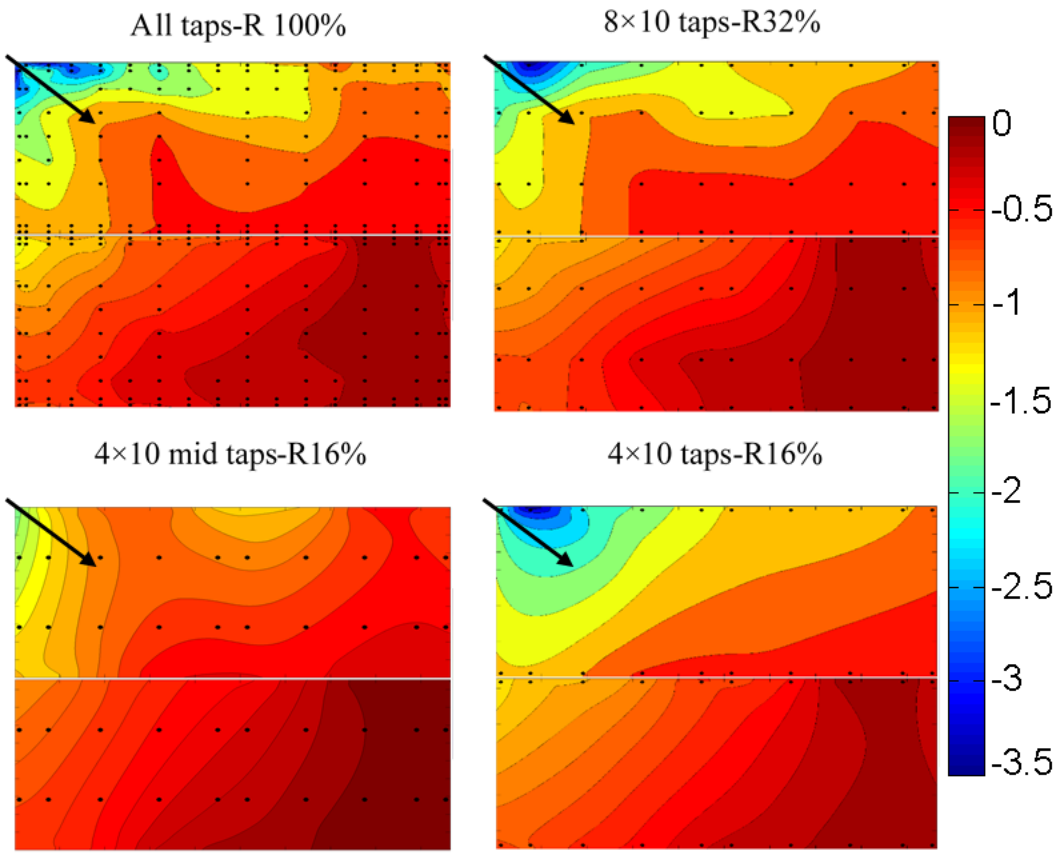

Figure 3.12: Net mean pressure coefficient (C_p) distribution of 135 degree wind angle of attack for different resolution

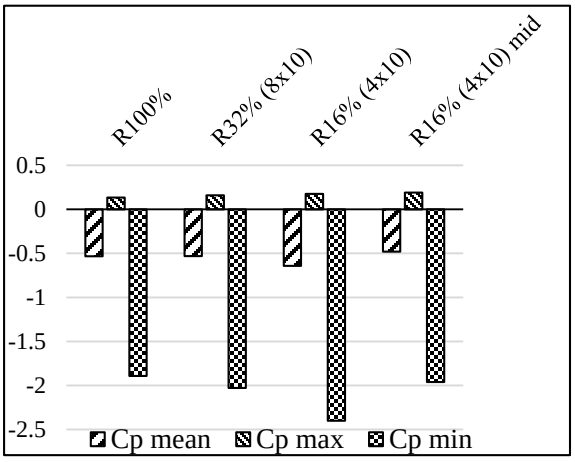

Figure 3.13: CPnet of different pressure tap layout for 135 degree wind angle of attack

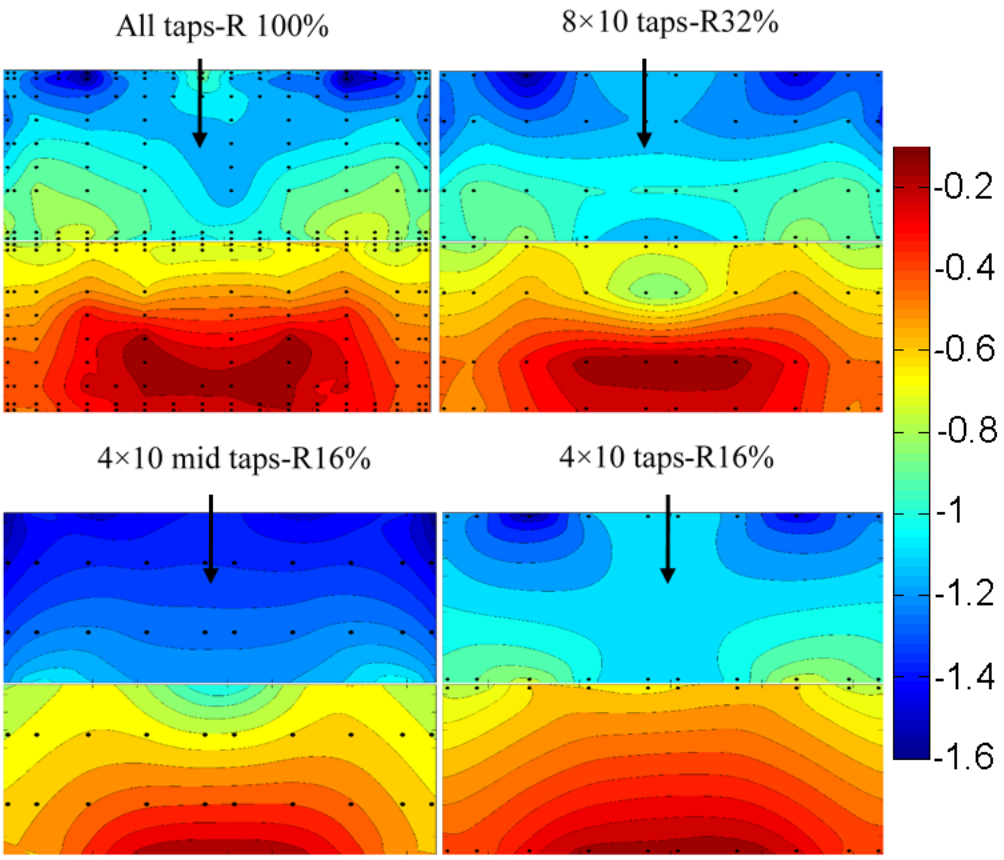

Figure 3.14: Net mean pressure coefficient (C_p) distribution of 180 degree wind angle of attack for different resolution

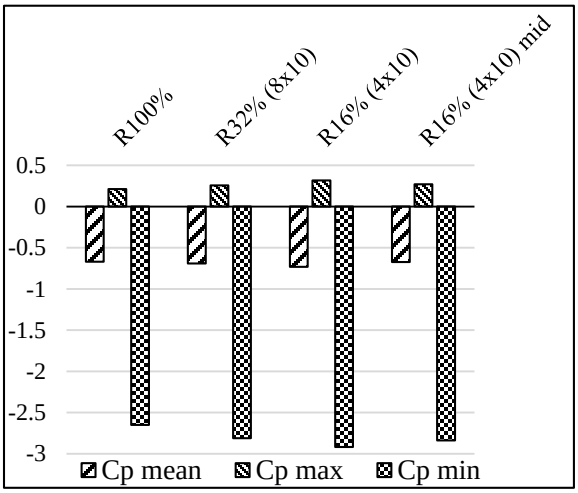

Figure 3.15: C_{Pnet} of different pressure tap layout for 180 degree wind angle of attack

3.5 Wind profile effect on pressure distribution

In order to understand the influence of the inflow conditions a comparison of mean net pressure coefficient contours obtained from boundary layer wind profile and uniform flow are plotted in Figure 3.16 for 0 degree wind angle of attack. It can be observed that the pressure distribution in both graphs are almost identical but the values are totally different. As expected, the net pressure coefficient achieved in uniform flow is almost 25% higher than those obtained in a boundary layer wind tunnel. The difference is more pronounced in Panel-2 (bottom panel) which is closer to the floor and turbulence of the floor roughness.

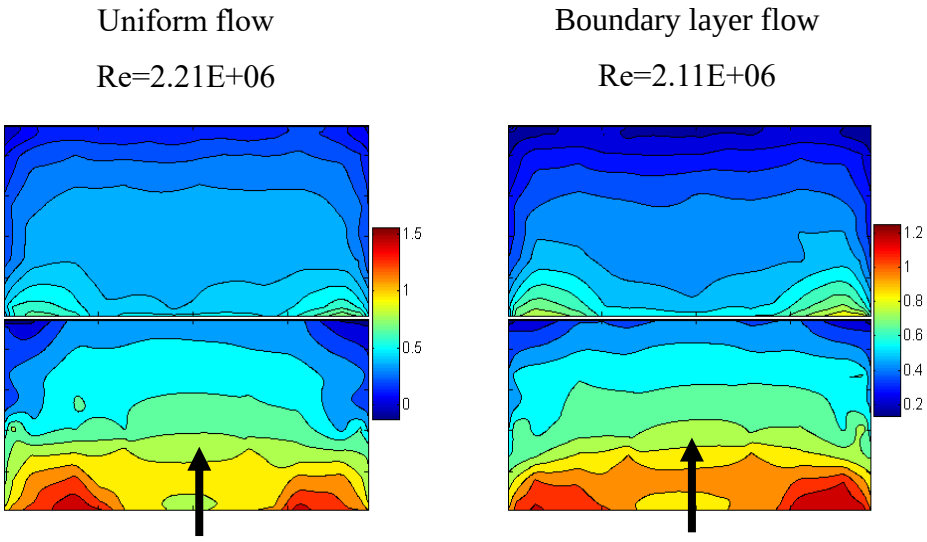

Figure 3.16: Comparison of Cp_{net} contour plots obtained from boundary layer and uniform flow for 0 degree wind direction

Note that the Reynolds numbers for boundary layer wind profile and uniform flow are also slightly different, as shown in Table 3.1 using Equation 3.3.

$$R_e = \frac{\rho v L p}{\mu} \qquad (3.3)$$

where R_e is Reynolds number, Lp is width of the panel (1.99 m), V is free stream velocity (15.88 m/s for boundary layer and 16.66 m/s for uniform flow), ρ is air density for 20^{oC} (1.2 kg/m^3) and μ is dynamic viscosity of the air for 20^{oC} (0.000018 Pa.s).

Table 3.1: Reynolds number of boundary layer and uniform flow

Flow	Reference velocity (m/s)	Reynolds
boundary layer	15.88	2.11E+06
uniform	16.66	2.21E+06

3.6 Force balance results

The same experimental analysis as described for solar panel model, is conducted on a real solar panel and the base reactions of the model for 0 to 180 degree wind angles of attack are obtained using the same boundary layer profile. For design purposes, the stability of the solar panel should be checked for drag force, lift force and overturning moment. To evaluate the effect of wind angle of attack, the base reactions are used for this analysis. To do so, normalized force coefficients of drag, uplift, downforce, and overturning moment are calculated using Equation 3.4 to 3.7.

$$(C_P C_g)_{drag} = \frac{F_{x,peak}}{(qC_e)A_{drag}} \tag{3.4}$$

$$(C_P C_g)_{uplift} = \frac{F_{z,\min,peak}}{(qC_e)A_{uplift}} \tag{3.5}$$

$$(C_P C_g)_{downforce} = \frac{F_{z,\max,peak}}{(qC_e)A_{downforce}} \tag{3.6}$$

$$(C_P C_g)_{moment} = \frac{M_{y,peak}}{(qC_e)A_{drag}H} \tag{3.7}$$

where C_pC_g is force/moment coefficient for each direction, F is peak reaction obtained through force balances, A is area corresponding to each force coefficient, q is wind pressure and C_e is exposure coefficient.

The force/moment coefficient for critical wind angles of attack are calculated and summarized in Table 3.2. Given the experimental data and test geometry, the calculations

are undertaken for A_{drag} =1.45 m^2, A_{lift} = $A_{downforce}$ =3.4 m^2 and average wind dynamic pressure of 155 Pa.

The achieved results indicate that the stability control is more critical at 180^o wind angle of attack for all drag, down force and overturning, as expected. The overturning force coefficient increases as the wind angle of attack turns to transverse angles. The drag force coefficient is also more critical for the heads-on directions, however 150^o wind angle is the second most critical angle for stability control and design of the solar racks.

Table 3.2: Peak pressure coefficient load case

Wind AOA	Flow	Maximum peak			Minimum peak		
		(CpCg) drag	(CpCg) uplift	(CpCg) moment	(CpCg) drag	(CpCg) uplift	(CpCg) moment
0 degree	**Boundary layer, Zo=0.01**	1.41	1.27	1.35	-0.08	-0.02	0.19
30 degree	**Boundary layer, Zo=0.01**	1.04	1.18	1.33	0.31	-0.06	0.26
45 degree	**Boundary layer, Zo=0.01**	1.04	1.18	1.33	0.31	-0.06	0.26
135 degree	**Boundary layer, Zo=0.01**	1.2	1.41	3.37	-0.23	0.15	0.27
150 degree	**Boundary layer, Zo=0.01**	1.45	1.7	4.04	-0.28	0.25	0.47
180 degree	**Boundary layer, Zo=0.01**	1.7	1.71	4.09	-0.09	0.27	0.61

3.7 Comparison of drag force coefficient with ASCE-7

The drag force coefficient obtained from the experimental analysis is compared with the equivalent value specified in ASCE-7 [ASCE 2010] for the same wind profile. The wind pressure in ASCE-7 is obtained from the equation of $P= q_h G C_N$, where q_h is velocity pressure evaluated at mean roof height h, G is a gust effect factor and C_N is a net pressure coefficient. If the parameters are correctly selected, GC_N prescribed in ASCE is comparable with $C_P C_g$ in this study.

According to ASCE-7 Figure 30.8-1, “Monoslope free roofs for $\Theta \leq 45$ degree”, the ratio of $0.25 \leq h/L \leq 1$ (h is mean roof height (m) and L is horizontal dimension of building which measured in along wind angle of attack (m)), roof angle $\Theta = 25^{o}$, $C_N = 2.3$, $G = 0.85$, GC_N is equal to:

$GC_N = 0.85 \times 2.3 = 1.95$

The results of this comparison is shown in Table 3.3 which indicates that ASCE-7 offers a good estimation for the drag force applied on a solar panel which is conservative if the parameter are correctly chosen.

Table 3.3: Drag force Coefficient obtained from ASCE and maximum Cp from experimental analysis for 0 degree wind angle of attack

	C_pC_g
ASCE	1.95
Experimental	1.7

3.8 Comparison of force balanced data with pressure taps

In order to assess any resonant components of the wind loads that may not be captured by the pressure model accurately, a force balance test on the real solar panel is conducted. This represented an aero-elastic model test of the solar panel at full-scale owing to the large size of the WindEEE Dome test section. The force balances placed underneath the actual solar racks in order to measure the base reactions. From the force balance recorded data, peak and mean value of drag and lift force of the solar rack are obtained. These values can be also achieved using the pressure taps recorded data. The two are expected to be similar if the dynamic effects (e.g. resonance effect) are minimal. The values of drag and lift force obtained through the pressure tests and the force balance are compared for different wind angles of attack.

Statistical values (max, min, mean and rms) obtained from above mentioned approaches for drag and lift force are shown in Table 3.4 and 3.5, respectively. Similar to previous statistical analysis earlier explained in this study, all pressure taps time histories data point are added up together at each step, and then statistical values of the summation time history are obtained. The same method is followed for the force balances. Maximum and minimum values are calculated using the Gumbel distribution method considering the probability of non-exceedance equal to 95%. The below conclusions can be drawn from the presented results in Table 3.4 and 3.5:

- The comparison of drag force achieved from the pressure taps of R100% and force balance indicates that for heads-on direction (0 and 180 degree) the mean pressure resulted from both methods are relatively close.
- In oblique direction, however, drag and lift forces achieved from the two methods are not quite comparable. The reason behind this difference is the less capability of the pressure tap system in measuring the total pressures, particularly once the vortex formation is significant on the surface of panel which is more noticeable in oblique wind angles. The second source of error in this comparison is that although the applied wind force on the solar racks is deducted from the force balance reactions to be comparable with wind induced pressure on the panel, this adjustment might not be perfect especially in oblique wind angles of attack.
- The wind induced turbulence around all the components of the solar panel system (including support system and ballast) are fully considered in the force balance test. In addition, any dynamic effects resulting from the solar panel excitation are captured during the force balance test. Therefore, the reaction forces directly obtained from force balances are more reliable values compared to those obtained from the pressure taps.

The difference on the uplift between the force balance and the pressure test is very high. To pinpoint the reason behind this, a detail spectral analysis is conducted. Spectral plots for selected pressure taps, group of taps and the uplift measurements from the force balance are plotted and shown in the Appendix B. As can be clearly seen from the spectra of the force balance, there is a significant dynamic effect

(resonance components) that are captured. These are missing from the pressure test. This explains the differences between the pressure test and force balance. This also highlights the need to carry out this type of dynamic analysis to estimate the peak loads on solar panels in particular and other similar small structures in general.

Table 3.4: Validation and comparison wind induced drag force obtained from force balances and pressure taps

		Drag Force [N]					
		Force balance	Force balance	Force of pressure taps			
		Aero-elastic model	Aerodynamic model	Resolution			
				R 100% Layout-1	R32% Layout-2	R16% Layout-3	R16% mid Layout-4
0 degree	mean	136.3	143.5	132.8	134.1	137.9	132.5
	max	279.1	287.9	237.7	241.6	253.9	237
	min	16.7	37.2	64	62.4	64.1	59.8
	rms	141.4	148.1	135.7	137.1	141.1	135.6
45 degree	mean	39.3	49.8	94.7	94.4	88.9	96.9
	max	181.7	139.5	193.5	186.9	192	189.1
	min	119.8	47.8	27.8	27.5	21.9	27.7
	rms	50.4	56.7	97.6	97.4	92	99.9
135 degree	mean	91.8	81.9	144.3	143.9	173.9	139.2
	max	211.7	263.5	280.5	283.5	341.9	266.5
	min	52.7	82.8	72.8	74.8	85.8	61.4
	rms	99.8	89.8	157.9	157.5	190.4	142.5
180 degree	mean	138.7	137.7	172	177.3	187.9	184.8
	max	324.7	358.3	315.6	315.6	361.1	327.1
	min	109	120	104.9	104.9	100.5	104.6
	rms	146.5	144.5	187.3	187.3	204.8	188.1

Table 3.5: Validation and comparison wind induced lift force obtained from force balances and pressure taps

		Lift Force [N]					
		Force balance	Force balance	Force of pressure taps			
		Aero-elastic model	Aerodynamic model	Resolution			
				R 100% Layout-1	R32% Layout-2	R16% Layout-3	R16% Layout-4
0 degree	mean	303.7	341.9	284.5	287.4	295.6	284
	max	653.4	702.4	509.4	517.7	544.1	507.8
	min	88	64.2	137.2	133.7	137.5	128.1
	rms	314.3	351.2	290.8	293.8	302.3	290.5
45 degree	mean	234.5	265.6	202.8	202.4	190.6	207.7
	max	649.2	575.6	414.7	400.5	411.5	405.2
	min	24.2	38	59.5	58.9	46.9	59.4
	rms	246.1	274.8	209.2	208.7	197.1	214.1
135 degree	mean	344.4	281.3	331	330	398.9	298.3
	max	764.6	731.8	601.1	607.6	732.7	571
	min	79.1	106.3	156	160.4	183.8	131.5
	rms	356	295.8	338.3	337.4	408	305.3
180 degree	mean	410.9	373.5	394.7	394.7	431	396
	max	869.4	864.3	676.4	676.4	773.7	701
	min	139.6	134.7	224.8	224.8	215.4	224.1
	rms	423.9	387.1	401.4	401.4	438.9	403.1

3.9 Conclusions

This study provides a comprehensive analysis of wind effects on high resolution full-scale ground mounted solar panel as well as an aero-elastic model. In this study the effect of wind angles of attack in both open terrain and uniform flow is considered. The following conclusions can be drawn from the present experimental study:

- The pressure distribution on the model at 0^o and 180^o wind angles of attack are almost symmetric about the center line. The solar panel experience the most critical

positive and negative values in these two directions, respectively. There is a little variation between the two panels as a result of the gap presence. The 20 mm gap between the panels induces a variation in pressure distribution in the direction of the flow.

- In oblique wind angles of attack mean Cp values decrease diagonally on the surfaces of panels along the wind angle of attack. Mean Cp distributions of oblique angles illustrate a separated region for both 45^o and 135^o wind angles of attack which confirms possible existence of corner vortices. Suction pressure is more critical at the top panel for 135^o wind angle of attack compared to 45^o wind angle of attack.
- Study of equivalent pressure reveals that the maximum force occurs at 180^o. So the stability of the solar panel should be controlled in the most critical direction which is the transverse drag force (180^o). From this study it can be concluded that the mean pressure cannot solely represent the critical wind angle of attack, and maximum and minimum Cp contour plots are also required for general conclusions.
- The pattern of the net pressure coefficient of the 1:10 scaled solar panel model investigated by Aly et.al, (Aly and Bitsuamlak 2012) is in good agreement with the full scale solar panel model obtained in this study.
- The comparison study with Abiola-Ogedengbe et al. (2015) revealed that the presence of 20 mm gap between panels is influential in pressure distribution. We also found that the presence of the concrete ballasts in full-scale assembly and congestion of pressure tubes caused a blockage and turbulence in the direction of flow at 180^o which affected the results.
- Study of pressure tap layout and resolution illustrated that a fairly high density resolution is required to capture all the aerodynamic features of pressure on the solar panel surfaces. However, the pressure contour and equivalent pressure coefficients obtained by R32% are reasonably acceptable. It is also concluded that edge taps are more influential in better representation of contour plots while mid taps with the larger tributary area are more influential in accuracy of the pressure coefficient values. It is found that mean pressure is almost insensitive to the

resolution percentage, however, peak pressure coefficients (Cp_{min} and Cp_{max}) significantly vary with resolution change.

- Comparison of contour plots obtained from uniform flow and boundary layer flow revealed that the pressure distribution in both graphs are almost identical but the Cp value of uniform flow are considerably higher particularly close to the ground.
- Study of force reaction of a real solar panel confirmed that the stability control is more critical in 180^o wind angle of attack for all drag, downforce and overturning cases. Also, 150^o wind angle is the second most critical angle for stability control and design of the solar racks.
- Comparison of experimental result with ASCE-7 indicated that ASCE-7 offers a good estimation for the drag force applied on a solar panel if the parameter are correctly chosen.
- The spectral analysis of the force balance and pressure data indicates that force balance results are a more reliable method of measurement as captures all dynamic features of the wind loading.

Chapter 4

4 Finite Element Analysis and Design Improvement of Solar Racks

This chapter presents the numerical analysis conducted on the solar panel model. The main objective is to determine the internal stresses through the finite element analysis (FEA) of the commonly used structural system using high resolution critical wind loads. The aim is to assess if there is a possibility of reducing the size or thickness (gauge) of the cross sections and save materials and therefore costs. For this purpose, the wind loading from the pressure test is used as an input load in the finite element model (FEM) of the supporting structure of solar panel (solar racks). The FEM is initially calibrated by the reactions obtained from the force balances during the tests. The FEM is further analyzed for a design wind speed as per the National Building Code of Canada (NBCC 2010) under the critical wind loading. Using the critical aerodynamic loadings obtained through the WindEEE experiments, structural design and cross-section revisions of supporting structure are performed.

4.1 Finite Element Model

4.1.1 Model Geometry and material properties

The supporting structure of solar panel (solar rack) consists of cold-form aluminum cross sections which are bolted together with proprietary connections. This structure comprises two prefabricated racks with all of their elements welded together. The racks are connected with interconnecting elements and L-shaped connections which are bolted together and form the entire structure. The racks geometry is accurately measured using the real experimental model as shown in Figure 4.1.

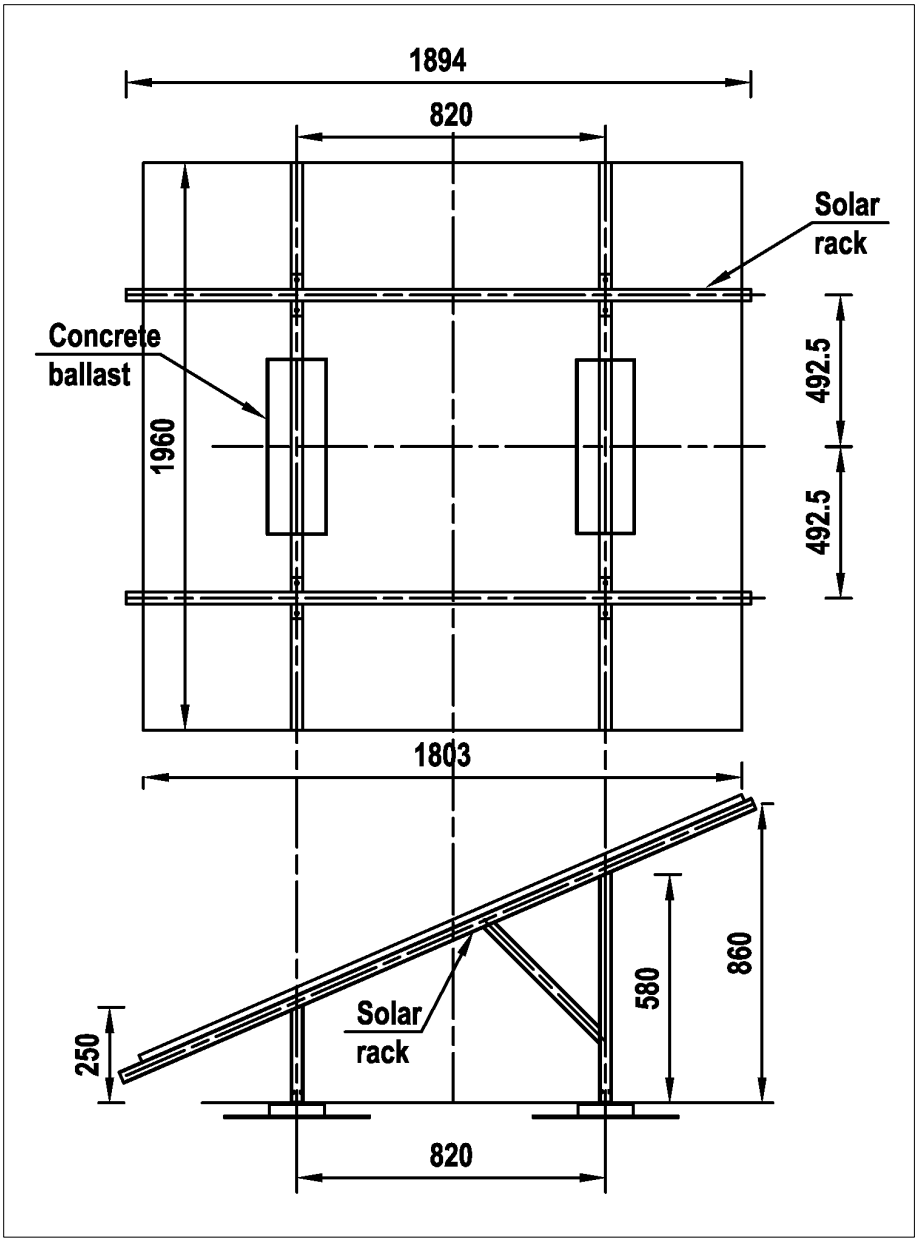

Figure 4.1: Plan and section view of the solar panel supporting structure

The elements of the racks are made of uni-strut cold formed aluminum sections called P1000, as shown in Figure 4.2. Uni-strut sections are typically formed from metal sheet, folded over into an open channel shape with inwards-curving lips to provide additional stiffness. These lips also provide a location to mount interconnecting components. The uni-strut cross section specifications are taken from the manufacturer data sheet of the racks as

shown in Table 4.1. The uni-strut of the racks are made of aluminum 6061-T6. The engineering characteristics are shown in Table 4.2.

The solar panel is placed in an aluminum frame which is clipped to the racks. The role of the panel in our FE model is to distribute the wind loading on solar racks. Hence, the stress analysis of the panel (solar cells) itself, is out of scope of this research. The panel is supported by two inclined rack elements and its connection to the rack is simulated similar to an aero-elastic model.

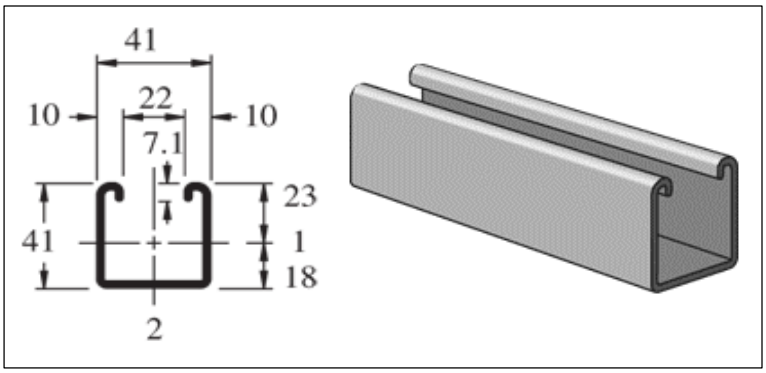

Figure 4.2: Cross section geometry of P1000 uni-strut

Table 4.1: Section properties of P1000 uni-strut

Elements of Section - P1000		
Element Material	Aluminium	
Depth of Section	41 mm	
Width of Section	41 mm	
Area of Section	360 mm^2	
	Axis 1-1	Axis 2-2
Moment of Inertia (I)	77000 mm^4	98000 mm^4
Section Modulus (S)	3300 mm^3	4800 mm^3
Radius of Gyration (r)	15 mm	17 mm

Table 4.2: Engineering properties of aluminum 6061-T6

Density	2700 kg/m^3
Elastic Modulus	69 GPa
Yield strength	270 MPa
Ultimate strength	310 MPa
Shear Strength	200 MPa

4.1.2 Elements simulation and boundary conditions

The FEM of the solar panel is simulated in the FEA software package SAP-2000 (CSI). The panel is modeled using finely meshed shell elements. The configuration of the panel is simulated by using a thin layer of glass (6 mm) with module of elasticity equal to 60 GPa. This approximation, although accurate enough, is done due to the absence of exact engineering characteristics of the panel material. The applied wind loading on the shell elements is transferred to solar rack members. The aspect ratio of the shell elements is kept closed to unity and limited to 2 for computational accuracy and better convergence.

The solar rack elements are modeled using 3D beam elements and fixed ends, which has 6 degrees of freedom at each end. Although the solar rack is basically a truss-like structure, all of the elements connections can withstand the bending moment as well, as they are either welded or bolted. The solar racks have four supporting points which are also modeled as fixed ends, as they are bolted to the interconnecting base elements. The finite element model of the solar panel is displayed in Figure 4.3.

For all the investigated wind angles of attack, i.e. 0, 45, 135 and 180 degree, the wind loading pressure is distributed on the shell elements. The maximum pressure applied on the panel is found at the instant that the pressure attains its peak value. The taps pressure distribution corresponding to that instance are applied on the panel and treated as maximum equivalent pressure. The steps of finding pressure distribution on the FE model are shown in Table 4.3. Assuming that the maximum value occurs at the time *m*, the pressures values

at this time for each taps (P_{nm}) is distributed on the panel of FE model at the location of the taps. The panel is discretized to 224 regions and the average of net pressure of the taps which are located on each division is applied on that area. The net peak pressure of each group of taps is calculated similar to the approach explained in Chapter 3, using Gumbel distribution statistical approach. Figure 4.4 shows the pressure distribution applied on the panel in FEM for 0 degree wind angle of attack. The minimal wind loading on supporting structure is not considered for the FEM analysis.

Table 4.3: Steps to find the instant that the pressure achieved its peak value

time history	**Load at tap #1**	**Load at tap #2**	**…**	**Load at tap #n**	**$F_t=\sum P_t \times A_n$**
t=1	$P_{11}\times A_1$	$P_{21}\times A_2$	…	$P_{n1}\times A_n$	$F_1=\sum P_{n1}\times A_n$
t=2	$P_{12}\times A_1$	$P_{22}\times A_2$	…	$P_{n2}\times A_n$	$F_2=\sum P_{n2}\times A_n$
.	.	.	…	.	.
t=m	$P_{1m}\times A_1$	$P_{2m}\times A_2$	…	$P_{nm}\times A_n$	$F_m=\sum P_{nm}\times A_n$
.	.	.	…	.	.
t	$P_{1t}\times A_1$	$P_{2t}\times A_2$	…	$P_{nt}\times A_n$	$F_t=\sum P_{nt}\times A_n$
					$F_{max}=MAX(F_t)$

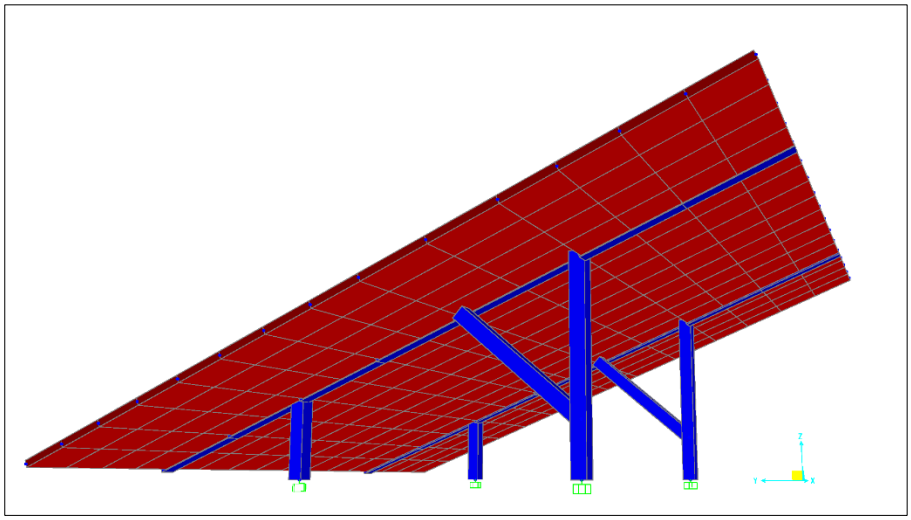

Figure 4.3: Finite element model of solar panel

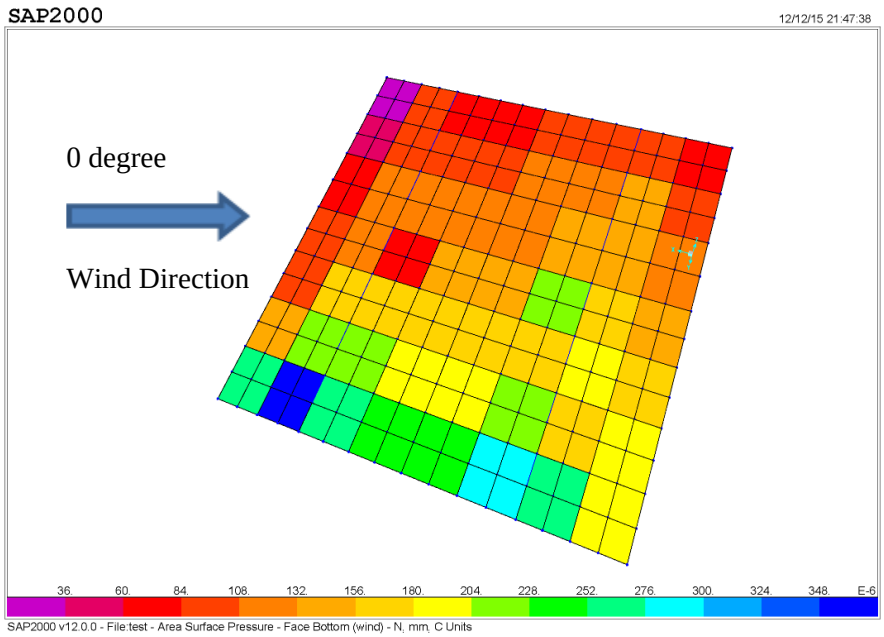

Figure 4.4: simulated wind pressure on solar panel FEM

4.1.3 Calibration of FE model

To ensure the accuracy of the FEM and before the application of the wind loading, the model is calibrated in two steps. In the first step, the weight of the model was checked and calibrated with the readings of the force balances without wind loading. The density of the panel and uni-struts are slightly adjusted in order to match with the real model. The second step is to check the stiffness of the model. During the experiment, two point loads are applied on the aero-elastic model at two different locations and the reactions of the solar rack are recorded through force balances, as displayed in Figure 4.5. Similarly, equal point load (20 kg) is applied on the FE model at the same location of the experimental model, and the reactions of the FE model are obtained. Results of this comparison are shown in table 4.4. The rear support reactions from FEA are added and compared with the readings of the rear force balance, excluding the weight of the concrete ballast. The obtained reactions from FEA are very close to those obtained by the force balances, indicating satisfactory simulation of the supporting structure.

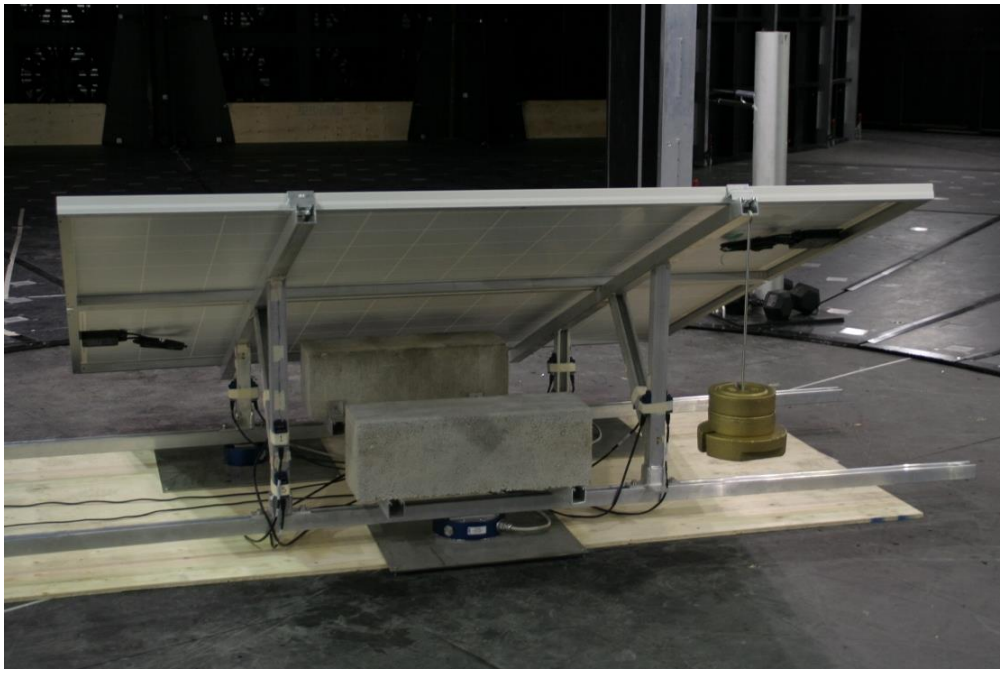

Figure 4.5: Calibration of the model

Table 4.4: Comparison of FEA support reactions with the experimental results obtained from force balances for 20 kg point load

		dead load base reactions (N)		
		Experimental	FEA (Fz)	
		With 20 kg point load	With 20 kg point load	
supports	front left	62.37	60.7	
	front right	84.73	81.2	
	rear left	636.9	415.5	614.12
	rear right		198.77	

4.1.4 FEA results and validation

Maximum equivalent net pressure is applied on the panel FEA for each wind angle of attack, as described in section 4.1.2. The wind induced reactions of the FE model are obtained and results are compared with experimental data. Table 4.5 shows the comparison of base reactions of the experimental and numerical analysis. The reactions obtained from

FE analysis are in agreement with the drag and lift forces obtained from the pressure tabs. This is due to the fact that the loading data of the FEA are acquired from the pressure tap results. In all cases, the difference of FEA results and pressure tap outcomes is between 4%-9%, indicating acceptable accuracy of finite element modeling. The source of this discrepancy is using average pressure on each mesh element of the solar panel. The difference can further be improved by using better pressure tributary areas and by improving the FE model representation.

Comparison of reactions of FE model with those obtained from force balance indicates 10-30% difference (see Table 4.5). The maximum differences are observed on the uplift forces. This is attributed to the additional aero-elastic forces that force balance is able to capture e.g. vibration of the panel but the pressure model is not. These are unique dynamic loadings that are observed while testing small structures in full-scale. These findings imply that dynamic analysis of these structures will be necessary to accurately assess their performance. These points are also discussed in Section 3.8.1.

Table 4.5: Comparison of FEA reactions with the experimental results obtained from pressure model and force balances

Wind direction	0 degree		180 degree		45 degree		135 degree	
Drag (Fx) and Lift (Fz) forces	Fx (N)	Fz (N)	Fx (N)	Fz (N)	Fx (N)	Fz (N)	Fx (N)	Fz (N)
SAP (FEA)	218	544	292	730	180	450	253	631
Pressure model	238	509	316	676	194	415	281	601
Force balance of real solar panel	279	653	324	869	182	649	212	765

4.1.5 Analysis and design of FEM under real wind loading

For the design improvement of the solar rack, a real value of the wind load should be applied on the panel considering the applicable load combinations as per NBCC (2010). All previous analysis were conducted based the reference wind speed equal to 15.88 m/s at WindEEE for an open terrain exposure. The design wind pressure for a return period of 50 years according to Appendix C (Climate data) of NBCC (2010), for London Ontario,

Canada area is V=28.9 m/s. Therefore, the real wind pressure in London area that should be applied on the FE model for design control of the solar panel elements is $(28.9/15.88)^2$= 3.31 times more than what is already applied on the panel in the experimental and numerical analysis. This is due to the fact that wind velocity correlates with pressure with power of two as indicated in Equation 1.2 and 1.3, where C_p is independent of wind velocity for high Reynolds number.

According to NBCC (2010) under Clause 4.1.3.2, the critical load combinations for design of solar panel supporting structure are as the following:

Case.1: 1.25×Dead load +1.4×Wind load

Case.2: 0.9×Dead load+1.4×Wind load

Where the first case governs the design of the uni-strut members and the second case governs the structural stability of the panel which is not part of the scope of this research

Another amplification factor is calculated based on the difference of force balance results and pressure taps and used for design improvement of rack elements. Since the force balances capture all dynamic features of the wind loading, their results are more reliable compared to pressure taps. Hence, the value of the pressure applied on FE model is adjusted using the amplification factor for each direction, however, the pressure distribution (Cp) is taken from the pressure taps and applied on the panel. This amplification factor is between 1.1 and 1.3 to adjust the 10-30% of the force achieved from the force balances and pressure taps.

The real wind pressure applied on the FEM of solar panel and the model is analyzed. Figure 4.6 shows the deflected shape of the solar panel under wind loading. Uni-strut members are then checked under the load combination of Case.1 for several wind directions. The design is conducted using aluminum design code, AA-LRFD 2000. In this code the aluminum resistance factor (Φ) is specified equal to 0.9.

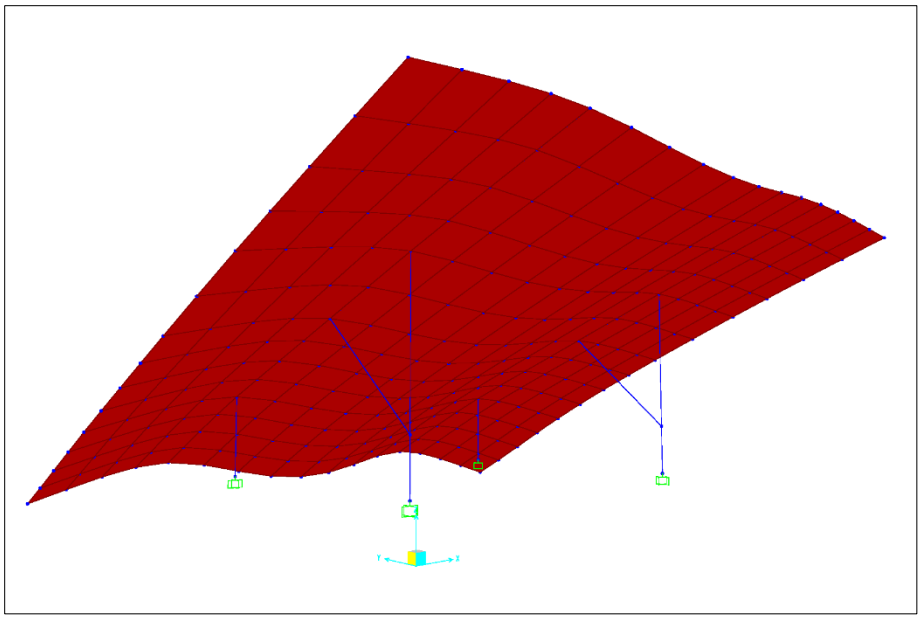

Figure 4.6: Deflected shape of the solar panel under wind loading (not to scale)

The results of the analysis show that the stress ratio (demand/capacity) of the P1000 uni-strut members does not exceed 0.25 for the critical elements. This means that all uni-strut elements have at least 75% more capacity. FEA results show that the maximum factored axial force is only 3.2 kN in the worst case. Manual calculations confirm that the results are in agreement with the manufacturing loading data shown in Table 4.6 which indicates that a 36in (910mm) uni-strut can carry 3190 lbs (14.2 kN) axial load. So the maximum stress ratio is 3.2/14.2=0.22 which reveals that the rack is considerably overdesigned. However, conducting dynamic analyses might be more accurate for final conclusions on the design of solar racks. Due to the small slope of the panel, all vertical elements of the rack (posts) are in tension for 180 degree wind direction and under compression for 0 degree wind direction. Since the maximum wind force occurs at 180 degree and the unbrace length of the posts are very short, the tensile stress ratio of the elements at 180 degree wind direction are more critical than compressive stress ratio at 0 degree.

Our analysis show that the deflection of the rack system under critical loading is not significant and is limited to 0.2 mm. It is currently unknown under what loading condition the rack was initially designed by the solar panel manufacturer. It is not clear if there is any other design criteria that should be considered for the design of uni-strut elements.

However, from structural perspective and based on static analyses, it appears that the current uni-strut are overdesigned and can be replaced with lighter sections.

Table 4.6: Capacity of P1000 uni-strut columns

Unbraced Height (in)	Allowable Load at Slot Face (lbs)	Max Column Load Applied at C.G.			
		K=0.65 (lbs)	K=0.80 (lbs)	K=1.0 (lbs)	K=1.2 (lbs)
24	3,550	10,740	9,890	8,770	7,740
36	3,190	8,910	7,740	6,390	5,310
48	2,770	7,260	6,010	4,690	3,800
60	2,380	5,910	4,690	3,630	2,960
72	2,080	4,840	3,800	2,960	2,400
84	1,860	4,040	3,200	2,480	1,980
96	1,670	3,480	2,750	2,110	1,660
108	1,510	3,050	2,400	1,810	×
120	1,380	2,700	2,110	×	×
144	1,150	2,180	1,660	×	×
×KL/r > 200					

4.2 Design of uni-strut elements

After several trial and error analysis, a lighter profile for uni-strut elements is selected and examined. This cross section, A1000, which is shown in Figure 4.7 is approximately 40% lighter than the original cross section P1000. The cross sectional properties of A1000 are shown in Table 4.7.

Using similar assumptions of the previous FE analysis, the solar panel is modeled using A1000 uni-strut elements and analyzed under different critical loading conditions. The wind loading was applied to the entire panel and the rack elements and the model was analyzed.

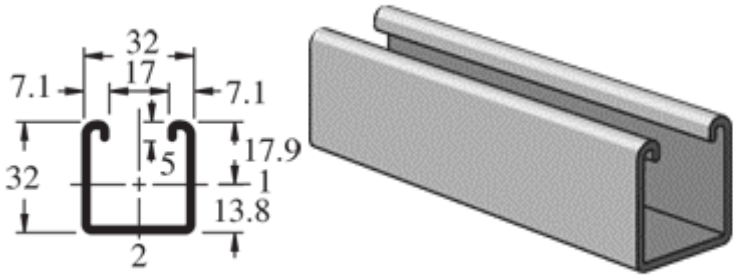

Uni-strut A1000 - 1-1/4" x 1-1/4"

Figure 4.7: Cross section geometry of A1000 uni-strut

Table 4.7: Section properties of A1000 uni-strut

Elements of Section - P1000		
	Axis 1-1	Axis 2-2
Moment of Inertia (I)	25000 mm^4	32000 cm^4
Section Modulus (S)	1400 mm^3	2000 cm^3
Radius of Gyration (r)	11 mm	13 mm

The stress ratio of the solar rack elements are shown in Figure 4.8. This figure demonstrates that the maximum stress ratio occurs at the inclined beam under the most critical wind loading (180 degree wind direction) where the stress ratio is 0.74. The maximum stress ration also occurs in the rear column equal to 0.44. The maximum deflection of the rack system in this case is 2 mm which is in an acceptable range.

The obtained results illustrate that using a lighter section for the racking system is more reasonable and economic, since the stress ratio is less than one. Results indicate that even a lighter uni-strut than A1000 can be used, however, the greater deflection of the panel might adversely affect the solar cells and their performance. This confirms the fact that the deflection control governs the design of solar rack rather than stress control.

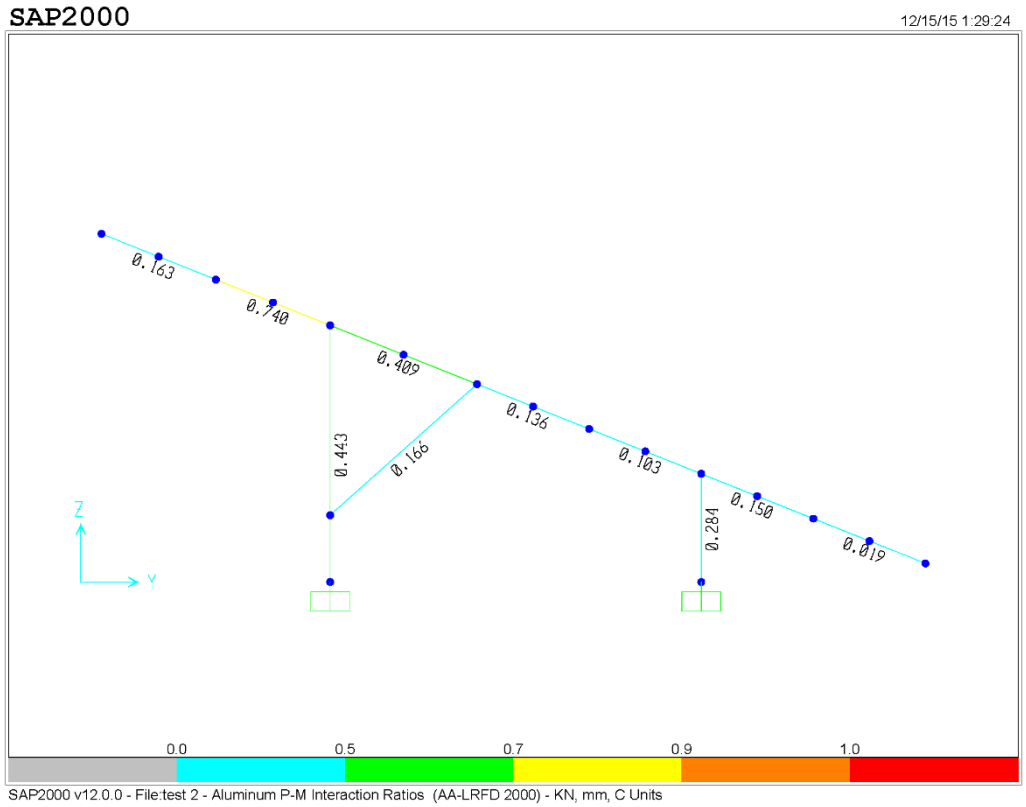

Figure 4.8: Stress ratios of the solar rack A1000 uni-strut elements under 180 degree wind direction

4.3 Discussion and Conclusion

The solar panel is modeled and examined under critical wind loading conditions obtained from the experimental analysis. The design of the original rack elements (P1000) is controlled as per AA-LFRD 2000, aluminum design code. The internal stress and deflection of members were obtained using the FEM simulated in SAP2000. It is concluded that the original uni-strut section is considerably overdesigned for southern Ontario cities such as London Ontario, Canada.

A lighter section, A1000 was replaced with the P1000 uni-strut the analysis and design were similarly performed. The results showed that using A1000 is structurally a feasible alternative to P1000 and leads to save in material up to 40%.

It should be noted that this conclusion is drawn solely based on the structural perspective. There might be other design considerations in terms of installation, manufacturing, thermal or electrical conductivity which govern the selection of the racking elements. However, the direct conclusion of this investigation is that P1000 is an overdesigned cross section of the solar panel system studied herein and using lighter elements is totally viable.

Chapter 5

5 Conclusions and recommendations

This chapter presents the summary of findings of the present work and suggests directions for future development. High resolution pressure tests under a realistically simulated turbulence ABL flow were conducted on full-scale solar panels with 25^o inclination in WindEEE Dome. Accurate pressure distributions on the solar panel were achieved for 21 wind directions (10-degree intervals from 0^o to180^o in addition to 45^o and 135^o) and the reactions of solar racks were obtained based on force balance tests. Sensitivity analyses were performed on both pressure and force measurements and the outcomes of both approaches are compared and discussed. A Finite element model of the solar panel was developed and the wind loading data obtained from wind testing was applied on the model. The design of the solar rack was evaluated and the internal stresses of the rack elements were determined under critical loading. This research established a better knowledge of wind effects on ground mounted solar panels which formed a base for design improvement of solar panel supporting structures.

5.1 Conclusions

Based on the tests and analysis performed through this study, it can be concluded that:

- The pressure distribution on the model at 0^o and 180^o wind angles of attack are almost symmetric about the center line. The solar panel experience the most critical positive and negative values for these two directions, respectively. There is little variation in pressure between the two panels as a result of the gap presence. The 20 mm gap between the panels induces a decline in pressure distribution in the direction of the flow.
- For oblique wind angles of attack mean Cp values decrease diagonally on the surfaces of panels along the wind angle of attack. Mean Cp distributions for oblique angles illustrate a separated region for both 45^o and 135^o wind angles of attack which confirms possible existence of corner vortices. The suction pressures are critical at the top panel for 135^o wind angle of attack compared to 45^o wind angle of attack.

- Study of equivalent pressure reveals that the maximum drag force occurs for 180^{o}. Therefore, the stability of the solar panel should be controlled in this direction which creates the critical drag force. From this study, it can be concluded that the mean pressure cannot solely represent the critical wind angle of attack, and maximum and minimum Cp contour plots are also required for general conclusions.
- The pattern of the net pressure coefficient of the 1:10 scaled solar panel model investigated by Aly et.al, (Aly and Bitsuamlak 2012) is in good agreement with the full scale solar panel model obtained in this study.
- The comparison study with Abiola et al. (Abiola-Ogedengbe et al., 2015) revealed that the presence of 20 mm gap between panels influences the pressure distribution.
- Study of pressure tap layout and resolution illustrated that a fairly high density resolution is required to capture all the aerodynamic features of pressure on the solar panel surfaces. However, the pressure contours and equivalent pressure coefficients obtained by R32% are reasonably acceptable. It is also concluded that edge taps are more influential in better representation of contour plots while mid taps with the larger tributary area are more influential in accuracy of the pressure coefficient values. It is found that mean pressures are almost insensitive to the resolution percentage, however, peak pressure coefficients (Cp_{min} and Cp_{max}) significantly vary with resolution change.
- Comparison of contour plots obtained for uniform flow and boundary layer flow revealed that their pressure distribution are almost identical, however, Cp values of the uniform flow are considerably higher particularly close to the ground.
- Study of base reactions of a real solar panel (aero-elastic model) confirmed that the stability control is more critical in 180^{o} wind angle of attack for all drag, downforce and overturning cases. Also, 150^{o} wind angle is the second most critical angle for stability control and design of the solar racks.
- Comparison of experimental result with ASCE-7 indicated that ASCE-7 offers a good estimation for the drag force applied on a solar panel if the parameter are correctly chosen.

- The spectral analysis of the force balance and pressure data indicates that force balance results are a more reliable method of measurement as it captures all dynamic features of the wind loading.
- For heads-on directions, the drag force obtained through force balances for both aero-elastic and aerodynamic model are almost identical in most of the cases, while for the lift force they are reasonably close. This can be attributed to the weight difference of the aero-elastic and aerodynamic model. As the aerodynamic model is lighter and more flexible in vertical direction, the lift force is subjected to more fluctuation. In Oblique direction, however, drag and lift forces achieved from the two methods are not directly comparable. The reason behind this difference is the lesser capability of the pressure tap system in measuring the total pressures particularly once the vortex formation is significant on the surface of panel which is more noticeable in oblique wind angles.
- The comparison of drag force achieved from the pressure taps of R100% and force balances indicates that for heads-on direction (0 and 180 degree) the mean pressure result from both methods are relatively close.
- FEA analysis showed that the reaction forces directly obtained from force balances are more reliable compared to those obtained from the pressure taps.
- The original uni-strut section (P1000) for the under-study solar panel system is considerably overdesigned for the wind loading in southern cities of Ontario such as London, and using lighter elements is totally viable.
- Using section A1000 is structurally a feasible alternative to P1000 and can lead to savings in material up to 40%.

5.2 Contributions

The original contributions of the present study to the scientific knowledge are provided below:

- Wind testing on a high resolution full-scale solar panel under a realistic simulated ABL flow are performed and sensitivity to tap distribution and density is determined.

- Detailed analysis of mean surface pressure coefficients was carried out in relation to the wind flow field around full-scale solar panels under 21 varying wind directions.
- The details of dynamic wind effects on the full scale panels of the supporting structure members are captured by using force balances.
- The cross section of the solar rack system was tentatively optimized by performing a finite element analysis.

5.3 Recommendations

Further improvement can be made in connection with the objectives of this study as the followings:

- The configuration of the rack system (supporting structure of solar panels) can be structurally optimized by changing the geometry and connections of the elements.
- Aerodynamic optimization of the panel can be performed to reduce the wind loads
- Strain gauges can be installed on the solar racks' elements in order to validate the stress ratio of the FEM.
- Dynamic wind analysis can be carried out to be compared with the experimental results.

References

Abiola-Ogedengbe, A., Hangan, H., Siddiqui, K., 2015. Experimental investigation of wind effects on a standalone photovoltaic (PV) module. Renewable Energy, 78, 657-665.

Abiola-Ogedengbe, Ayodeji, 2013. Experimental investigation of wind effect on solar panels. Thesis and Dissertation Repository, University of Western Ontario.

Aly, A.M., Bitsuamlak, G.T. 2014. Wind-induced pressures on solar panels mounted on residential homes, Journal of Architectural Engineering, ASCE, 20(1), 04013003

Aly, A.M., Bitsuamlak, G., 2013. Aerodynamics of ground-mounted solar panels: Test model scale effects. Journal of Wind Engineering and Industrial Aerodynamics 123, 250-260.

Aly, A.M., Bitsuamlak, G.T., Chowdhury, A.G., 2012. Full-scale aerodynamic testing of a loose concrete roof paver system. Eng. Struct. 44, 260–270.

ASCE 7-10, 2010. Minimum Design Loads for Buildings and Other Structures. ASCE 7-10, Virginia, USA: American Society of Civil Engineers.

Asghary Mooneghi, M., Irwin, P., Chowdhury, A.G., 2014. Large-scale testing on wind uplift of roof pavers. Journal of Wind Engineering and Industrial Aerodynamics 128, 22-36.

Bitsuamlak, G. T., Dagnew, A. K., Erwin, J., 2010. Evaluation of wind loads on solar panel modules using CFD. The Fifth International Symposium on Computational Wind Engineering, Chapel Hill, North Carolina, USA, May 23-27.

Engineering Data Science Unit, Strong winds in the atmosphere boundary layer. Part 1: Mean-hourly wind speeds, Data Item 82026, 1982.

Engineering Data Science Unit, Strong winds in the atmosphere boundary layer. Part 2: Turbulence intensity, Data Item 83045, 1983.

Fage, A., Johansen, F. C., 1927. On the flow of air behind an inclined flat plate of infinite span. Proceedings of the Royal Society of London. Series A, Containing Papers of a Mathematical and Physical Character 116, 170-197.

Hangan, H., 2010. Current and Future Directions for Wind Research at Western: A New Quantum Leap in Wind Research through the Wind Engineering, Energy and Environment (WindEEE) Dome. Wind Engineers, JAWE, Vol. 35, No.4.

Hangan, H., 2014. The Wind Engineering Energy and Environment (WindEEE) Dome at Western University, Canada. Wind Engineers, JAWE, Vol. 39, No.4.

Hosoya, N., Peterka, J. A., Gee, R. C., & Kearney, D. 2008. Wind Tunnel Tests of

Parabolic Trough Solar Collectors. NREL/SR-550-32282, May 2008, Golden, Colorado:

National Renewable Energy Laboratory.

Jubayer, C. M., Hangan, H., 2014. Numerical simulation of wind effects on a stand-alone ground mounted photovoltaic (PV) system. Journal of Wind Engineering and Industrial Aerodynamics. 134, 56–64.

Kopp, G. A., Banks, D., 2013. Use of wind tunnel test method for obtaining design wind loads on roof-mounted solar arrays. Journal of Structural Engineering 139, doi: 10.1061/ (ASCE) ST.1943-541X.0000654.

Kopp, G. A., Farquhar, S., Morrison, M. J., 2012. Aerodynamics mechanisms for wind loads on tilted, roof-mounted, solar arrays. Journal of Wind Engineering and Industrial Aerodynamics 111, 40-52.

Menter, F. R., 1994. Two-equation eddy-viscosity turbulence models for engineering applications. American Institute of Aeronautics and Astronautics (AIAA) Journal 32, 1598-1605.

NBCC, 2010. Canadian Commission on Building and Fire Codes National Research Council of Canada. National Building Code of Canada, Ottawa.

SAP2000. Structural Analysis Program. Computers and Structures, Inc. United states, Berkley, CA.

Shademan, M., Hangan, H., 2010. Wind loading on solar panels at different azimuthal and inclination angles. The Fifth International Symposium on Computational Wind Engineering, Chapel Hill, North Carolina, USA, May 23-27.

Shademan, M., Barron, R. M., Balachandar, R., Hangan, H., 2014a. Numerical simulation of wind loading on ground-mounted solar panels at different flow configurations. Canadian Journal of Civil Engineering 41, 728-738.

Shademan, M., Balachandar, R., Barron, R. M., 2014b. Detached eddy simulation of flow past an isolated inclined solar panel. Journal of Fluids and Structures 50, 217-230.

Shih, T. H., Liou, W. W., Shabbir, A., Yang, Z. And Zhu, J., 1995. A new k-eddy-viscosity model for high Reynolds number turbulent flows model development and validation. Computers & Fluids 24, 227-238.

Stathopoulos, T., Zisis, I., Xypnitou, E., 2014. Local and overall wind pressure and force coefficients for solar panels. Journal of Wind Engineering and Industrial Aerodynamics 125, 195-206.

Tieleman, H.W., Reinhold, T.A., Hajj, M.R., 1997. Importance of turbulence for the prediction of surface pressures on low-rise structures. Journal of Wind Engineering and Industrial Aerodynamics 69(71), 519–528.

Warsido, W., Bitsuamlak, G.T., Gan Chowdhury, A., Barrata, J. 2014. “Influence of spacing parameters on the wind loading of solar array”, Journal of Fluids and Structure, 48, 295–315.

Appendices

Appendix A: Equivalent pressure coefficient for all wind angles of attack

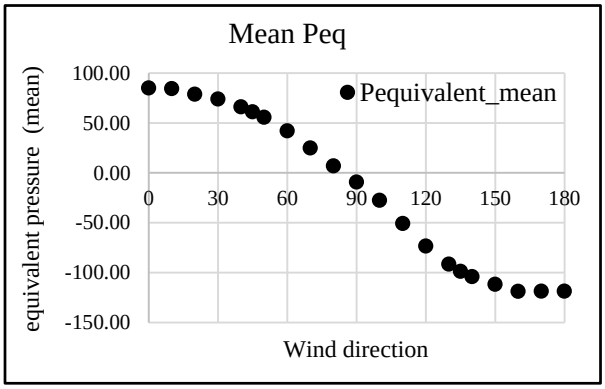

(a)

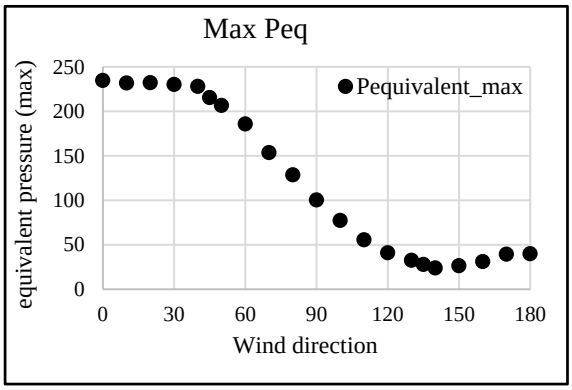

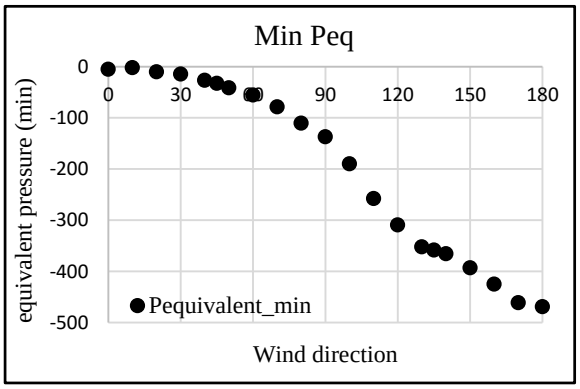

(b) (c)

Figure A.1: (a) Mean, (b) maximum and (c) minimum equivalent pressure for all wind angles of attack

Appendix B: Spectra of net pressure of pressure taps and force balances

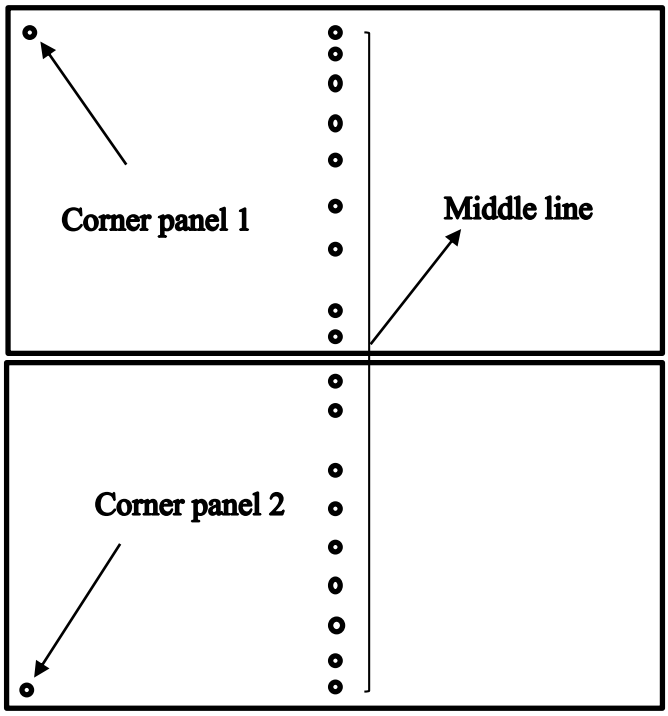

Figure B.1: Location of the pressure taps on the panels used for normalized spectra

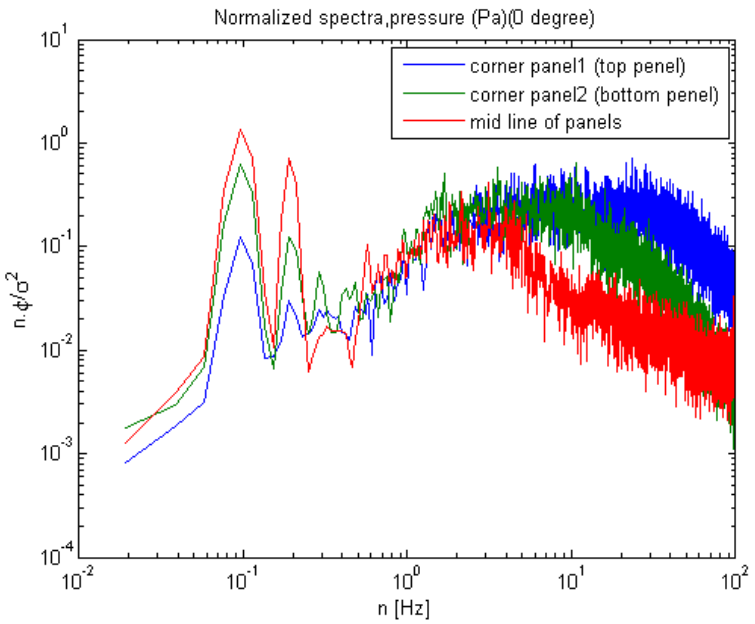

(a)

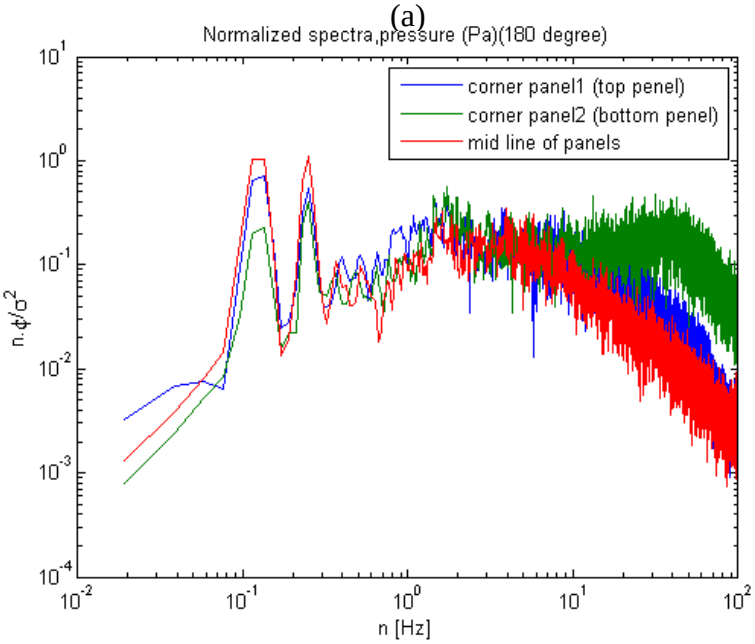

(b)

Figure B.2: Normalized spectra of net pressure at the corner and middle line for (a) 0 degree and (b) 180 degree wind angle of attack

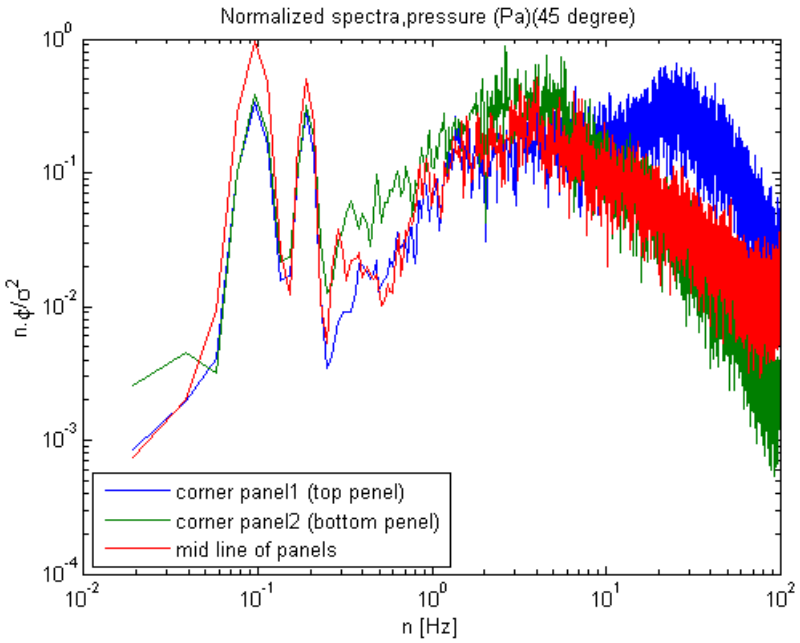

(c)

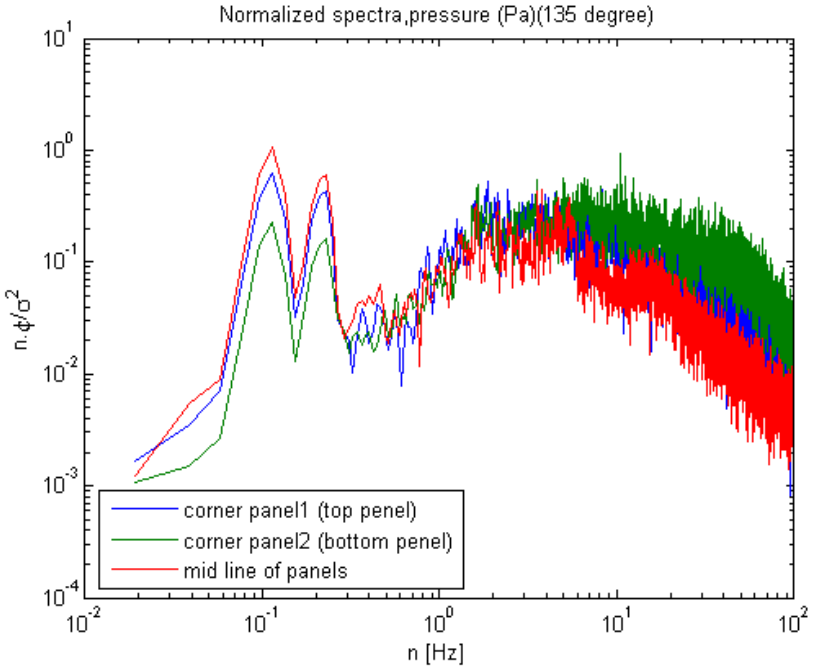

(d)

Figure B.3: Normalized spectra of net pressure at the corner and middle line for (a) 45 degree and (b) 135 degree wind angle of attack

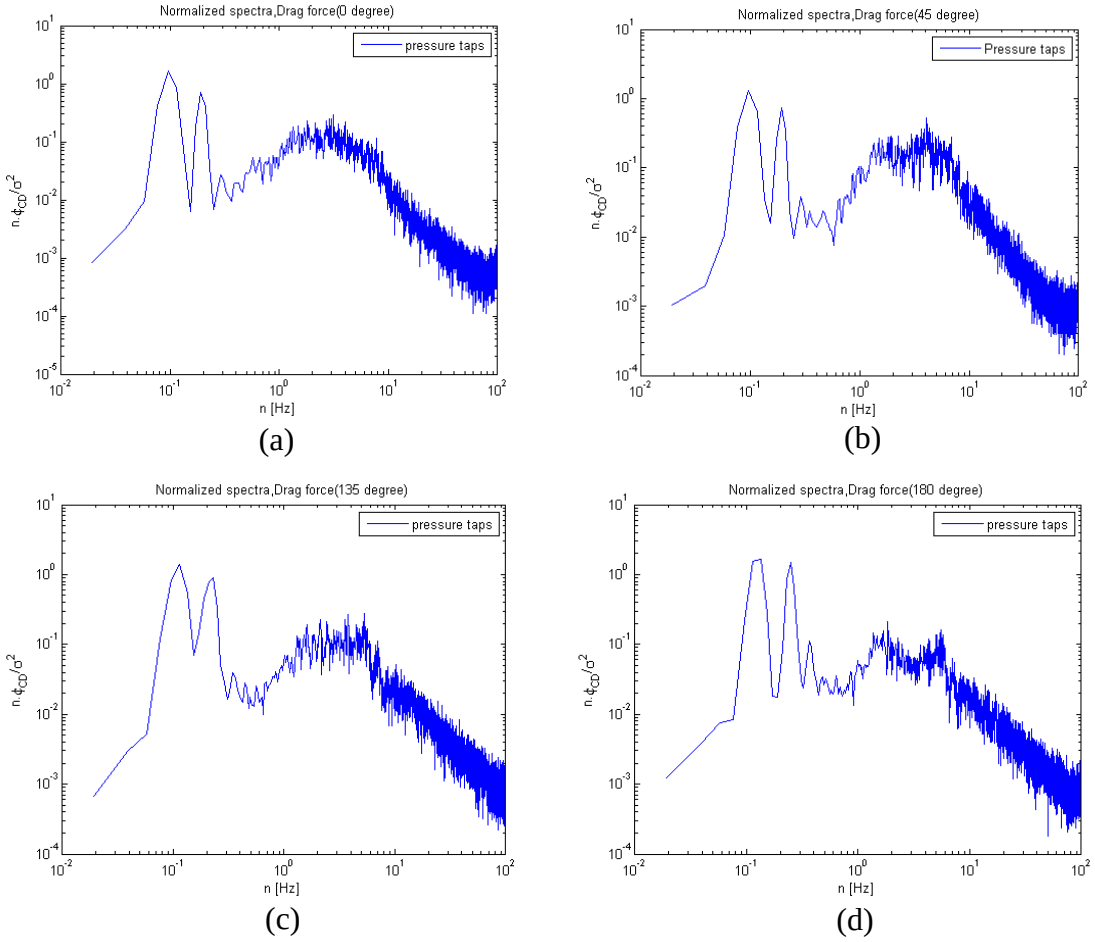

Figure B.4: Normalized spectra of drag force from pressure taps for (a) 0 degree, (b) 45 degree (c) 135 degree and (d) 180 degree wind angle of attack

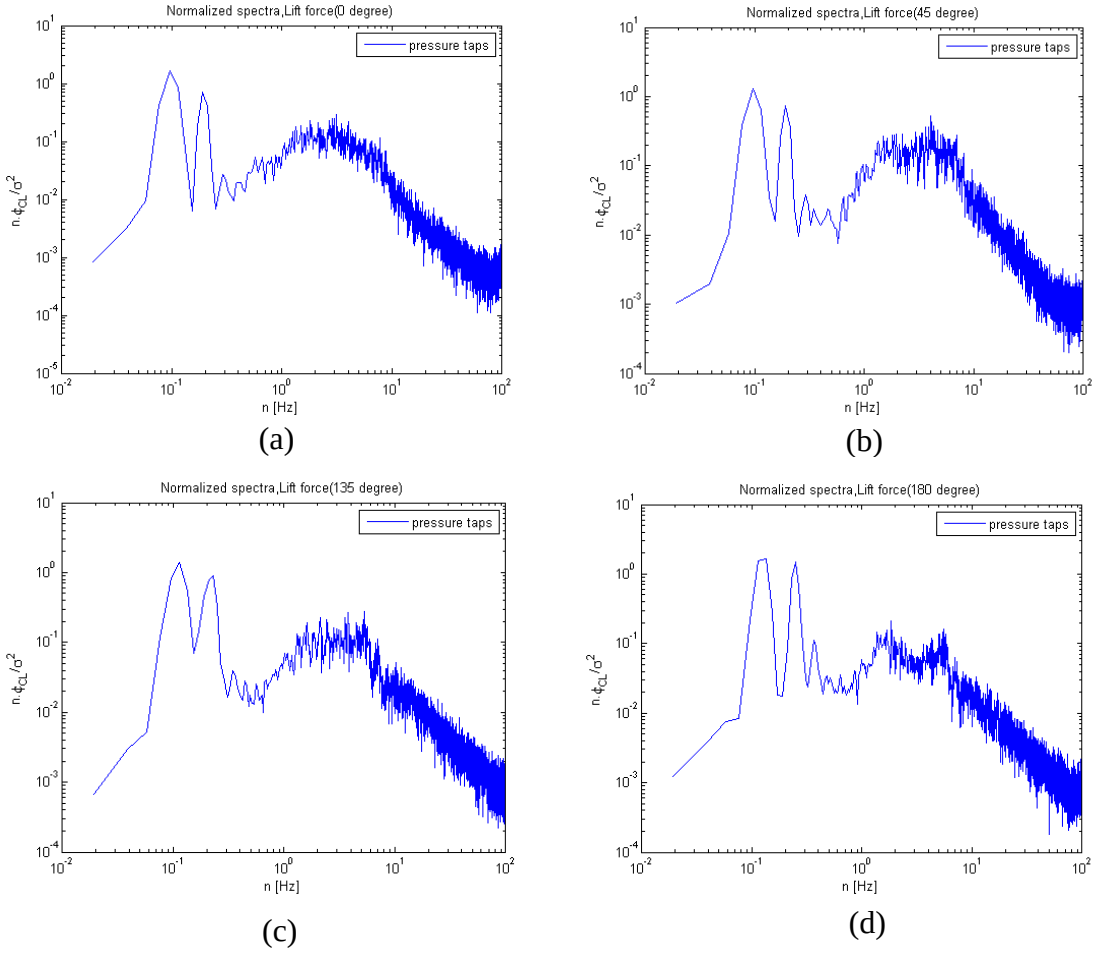

Figure B.5: Normalized spectra of lift force from pressure taps for (a) 0 degree, (b) 45 degree (c) 135 degree and (d) 180 degree wind angle of attack

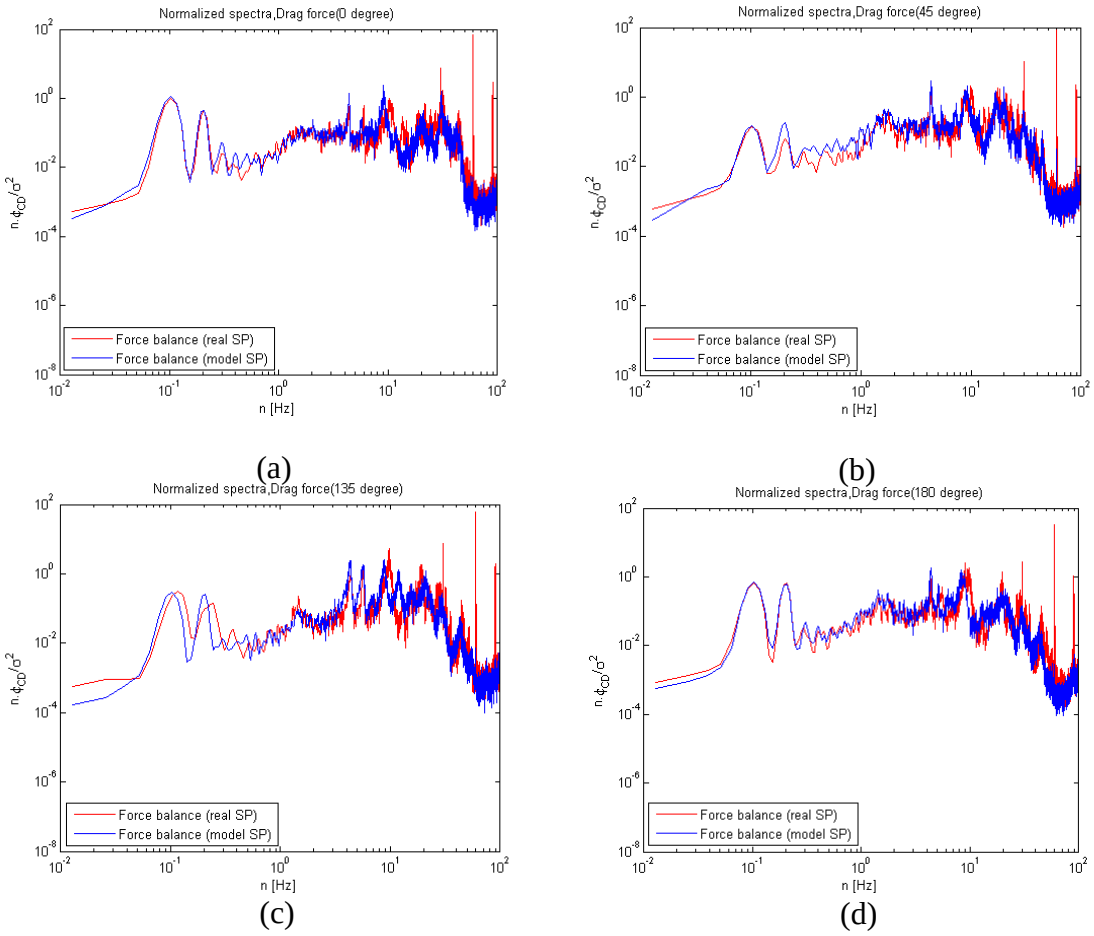

Figure B.6: Normalized spectra of drag force from force balances of the model and real solar panel for (a) 0 degree, (b) 45 degree (c) 135 degree and (d) 180 degree wind angle of attack

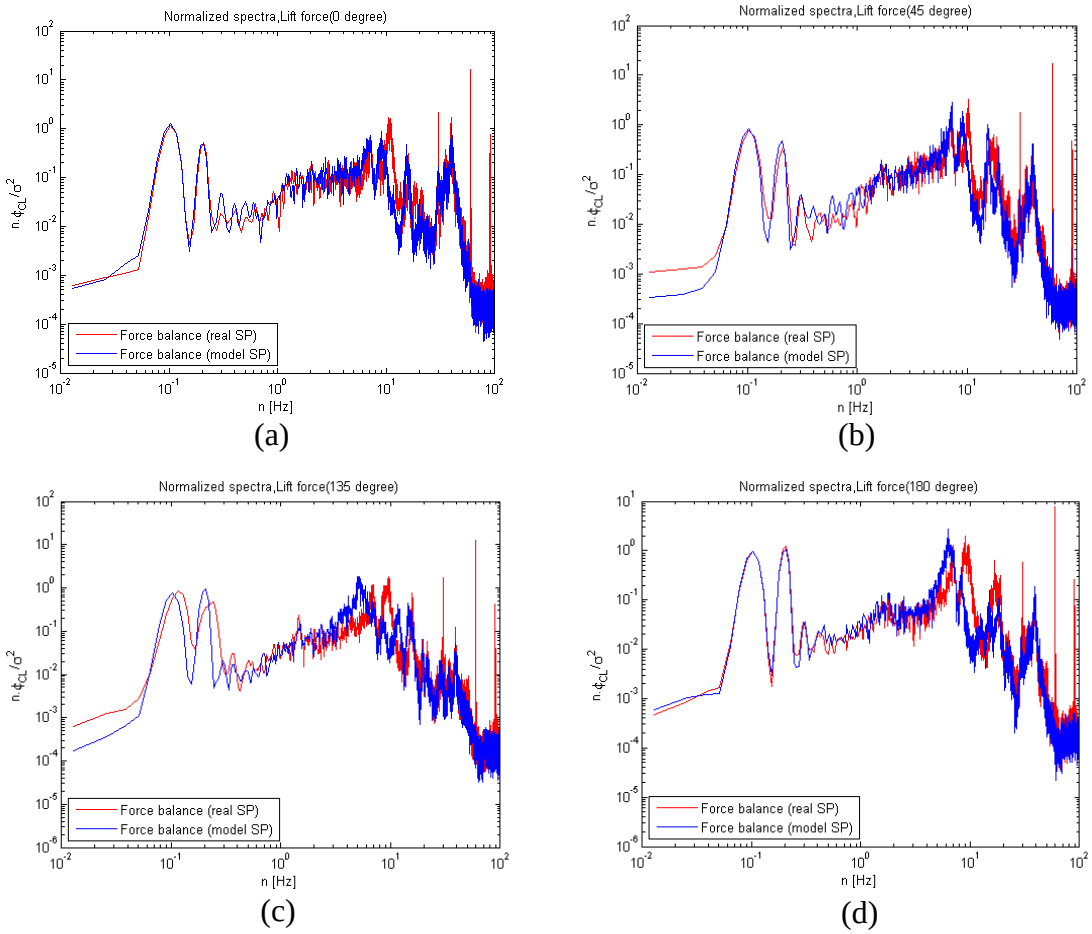

Figure B.7: Normalized spectra of lift force from force balances of the model and real solar panel for (a) 0 degree, (b) 45 degree (c) 135 degree and (d) 180 degree wind angle of attack

Curriculum Vitae

Name: Zeinab Mohammadvali Samani

Post-secondary Education and Degrees:

The University of Western Ontario
London, Ontario, Canada
2014-2016 MESc.

The University of Tehran
Tehran, Iran
2008-2010 MESc.

Shahid Chamran University
Ahvaz, Iran
2002-2006 B.A.

Honours and Awards:

Western Graduate Research Scholarship
2014-2015

Top Student Award
2005

Related Work Experience

Teaching Assistant
The University of Western Ontario
2014-2015

Research Assistant
The University of Western Ontario
2014-2015

Publications:

- Haghighi, A., Mohammad, H., Samani, Z., 2011. GA-ILP Method for Optimization of Water distribution Networks. Water Resources Management, Vol.25. N.7. P.1791-1808.